Finanziato dall'Unione europea NextGenerationEU
Ministero dell'Università e della Ricerca
Italiadomani PIANO NAZIONALE DI RIPRESA E RESILIENZA

multi-Risk sciEnce for resilienT commUnities undeR a changiNg climate
Codice progetto MUR: **PE00000005** – CUP LEAD PARTNER: I33C22006910006

Deliverable title: Natural Hazards classification maps of individual network of linear infrastructures – Methodology Report

Deliverable ID: DV 6.3.1

Due date: February 2025

Submission date: February 2025

AUTHORS

Pierluigi Claps, Daniele Ganora, Paola Mazzoglio, Giulia Evangelista (POLITO), Francesco Napolitano, Elena Ridolfi, Benedetta Moccia (UNIROMA1), Salvatore Manfreda, Jorge Andres Saavedra Navarro, Angelo Avino (UNINA), Eva Trasforini, Tatiana Ghizzoni, Bruno Colavitto (CIMA), Laura Longoni, Matteo Antelmi, Monica Corti, Lorenzo Panzeri (POLIMI), Paolo De Girolamo, Carolina Codato (UNIROMA1), Lisa Borgatti, Giacomo Titti, Davide Donati (UNIBO), Giorgio Bellotti, Alessandro Romano, Leopoldo Franco, Claudia Cecioni (UNIROMA3), Pasquale Fabio Giuseppe Filianoti (UNIRC), Marcello Di Risio, Davide Pasquali (UNIVAQ).

Approved by Paola Mazzoglio (WP leader)

1. Technical references

Project Acronym	RETURN
Project Title	multi-Risk sciEnce for resilienT commUnities undeR a changiNg climate
Project Coordinator	Domenico Calcaterra UNIVERSITA DEGLI STUDI DI NAPOLI FEDERICO II domcalca@unina.it
Project Duration	December 2022 – November 2025 (36 months)

Deliverable No.	DV6.3.1
Dissemination level*	PU
Work Package	WP3 - Dynamic mapping of natural and climatic hazards over the infrastructure systems
Task	T3.1 - Robust hazard mapping over network infrastructures (link with Spokes 1÷3)
Lead beneficiary	POLITO, UNIROMA1
Contributing beneficiary/ies	POLITO, UNIROMA1, UNINA, CIMA, POLIMI, UNIBO

* PU = Public

PP = Restricted to other programme participants (including the Commission Services)

RE = Restricted to a group specified by the consortium (including the Commission Services)

CO = Confidential, only for members of the consortium (including the Commission Services)

Document history

Version	Date	Lead contributor	Description
0.1	05.02.2025	UNIROMA1 e POLITO	First draft
0.2	15.02.2025		Critical review and proofreading
0.3	20.02.2025		Edits for approval
1.0	28.02.2025		Final version

2. Abstract

Within Task 3.1, dynamic mapping was conducted to reflect the evolving knowledge evolution of the hazard assessment derived from Spokes 1 to 3. The mapping criteria stem from existing robust and reliable methodologies ensuring a reliable classification of hazards affecting key transport and utility infrastructure, including roads, railways, waterways, and the utility grid.
This Task produced methodologies for hazard assessment and natural hazard classification maps for linear infrastructures in the following domains: extreme rainfall (Section 3.1.a), floods (Section 3.1.b), coastal flooding induced by extreme wind waves (Section 3.1.c) and landslides (Section 3.1.d).
This deliverable outlines the products that were developed within Task 3.1 of the Spoke TS2 to achieve these objectives, which can be summarized as follows:

- up-to-date high-resolution national-scale maps of extreme rainfall statistics (Section 3.1.a);
- national-scale inventory of 631 gauged basins with over 100 attributes related to geomorphology, soil, land cover, vegetation, climate, and extreme precipitation (Section 3.1.a);
- methodology for reliably estimating basin flood response time to develop design flood hydrographs in ungauged basins (Section 3.1.a);
- guidelines for evaluating flood-related hazard based on watershed characteristics and on the infrastructure section type (Section 3.1.b);
- national/regional flood scenarios that integrate satellite-derived flood maps and historical flood data in combination with geomorphic basin features and climatic conditions features as inputs for machine learning models (Section 3.1.b);
- a probabilistic risk assessment for isolated areas at regional scale (Section 3.1.b);
- the estimation of coastal flooding areas, induced by extreme waves and water level conditions, with an innovative methodology capable of considering potential MeteOcean scenarios altered by climate changes (Section 3.1.c);
- evaluation of the landslide hazard at a regional scale and its interaction with linear infrastructures, but in current and future scenarios of landslide occurrences (Section 3.1.d).

The second part of the deliverable will instead focus on the implementation process and the key results obtained.

3. Table of contents

List of Figures

3.1 Natural Hazards classification maps of individual network of linear infrastructures

3.1.a Increasing the spatial detail of the hydrological hazard mapping

3.1.a.1 FOCA dataset

3.1.a.1.1 Introduction

The availability of complete, updated and quality-controlled hydro-geomorphological information for areas nationwide is a key requirement for a vast range of applications from hydrological modeling to hydraulic simulations and rainfall-runoff analyses. Hydro-geomorphological catchment information, also called *catchment attributes*, can also provide a comprehensive description of the landscape and of how the catchment stores and transfers water (Addor et al., 2017).

In recent years, considerable efforts have been dedicated to producing similar datasets at the national scale. Relevant examples are the datasets built in the framework of the CAMELS (Catchment Attributes and MEteorology for Large-sample Studies) initiative, as in the cases of Great Britain, France, Switzerland, Germany, the United States, Chile, Brazil, and Australia. Most of those datasets have since been linked together to build the Caravan dataset (Kratzert et al., 2023). Other large-scale datasets have been developed independently of the CAMELS framework, such as those related to China (Hao et al., 2021) and to the area of the upper Danube up to the Austria–Slovakia border and some nearby catchments (Klingler et al., 2021).

As of today, only partial-coverage datasets (in terms of both spatial extent and the number of variables) are available for Italy. A complete and updated database of hydro-geomorphological variables relating to the main catchments of Italy is missing. One of the reasons behind this gap is the dismantlement of the National Mareographic and Hydrographic Service (Servizio Mareografico e Idrografico Nazionale, SIMN), which has led to the federated management of the national monitoring network by 21 different administrative agencies. In this work, we present FOCA (Italian FlOod and Catchment Atlas; Claps et al., 2024), a collection of attributes of 631 Italian river catchments derived from data sources that comply with the following criteria: i) nationwide coverage; ii) consistency in data quality (i.e., no regional or local biases); and iii) adequate original resolution in relation to the type of information. FOCA represents the most up to date collection of catchment boundaries and related attributes at the national scale for Italy. It summarizes features related to climate (discharge, rainfall and temperature), geomorphology, soil and land use. The dataset covers an overall area representative of most of the landscapes of Italy, including the mountainous ones (elevations ranging from 0 to 4800 m). One of the main novelties with respect to other national-scale datasets is the inclusion of a rich set of geomorphological and extreme rainfall attributes. The second notable novelty is the inclusion, in the same dataset, of the most up to date information regarding extreme rainfall and discharge.

3.1.a.1.2 Presentation of historical catalogs and the rationale for catchment selection

Since the early 1990s, the Italian monitoring network was managed by the SIMN. This institution was in charge of the collection and validation of the data and its publication in a series of hydrological yearbooks with yearly updates. To facilitate access to the discharge data, this information was then processed by the SIMN at monthly time resolution and grouped by individual gauging station with the aim of providing several years of data on one data sheet for each station. This summarized information, available up to 1970 and complemented with some basic catchment information, became *Pubblicazione no. 17* (Publication no. 17). The interruption of the publication of *Pubblicazione no. 17* had a particularly negative effect on access to the peak discharge data: these measurements were only published in *Pubblicazione no. 17* as the maxima of the instantaneous discharge and have never been available in the hydrological yearbooks. The main effort to recover these unpublished data was made by the GNDCI (Gruppo Nazionale per la Difesa dalle Catastrofi Idrogeologiche) as part of the VAPI (VAlutazione delle PIene) project

(http://www.idrologia.polito.it/gndci/Vapi.htm), which was subsequently integrated into the CUBIST project. In the following years, some regional-scale works were conducted to update this systematic collection but without nationwide coordination. Only in recent years, the different flood datasets were homogenized, integrated and updated by including the most recent data acquired across Italy, leading to the release of a comprehensive catalog of floods (Catalogo delle Piene dei Corsi d'acqua Italiani; Claps et al., 2020a, 2020b, 2020c). However, in this case, only basic geomorphological information was included for the considered basins. The catchment selection criterion adopted in the present work stems from the purpose of improving upon the work reported in Claps et al. (2020a, b, c). The 631 chosen catchments are those for which peak or daily discharges are available and are therefore all included in Claps et al. (2020a, b, c).

3.1.a.1.3 Data and catchment geomorphological attributes

In this work, we adopted the DEM from the Shuttle Radar Topography Mission (SRTM) at 30 m spatial resolution (Farr et al., 2007). The processing of the DEM and, in general, all the other catchment attributes was performed with open-source software, namely GRASS GIS and R.

DEMs usually contain pits (i.e., elevation values that are much lower than those of nearby pixels; these are errors due to the resolution of the data) that should be filled to ensure the proper delineation of catchment boundaries and drainage networks. Thus, the pit-filling procedure was carried out using the r.hydrodem add-on for the GRASS GIS (Lindsay and Creed, 2005).

To determine the basin boundaries, it is first necessary to generate the drainage network from the depitted DEM. This step can be done only once with the r.basin command and involves the following steps: (i) the calculation of the drainage directions with the multiple flow direction (MFD) algorithm; (ii) the calculation of the flow accumulation, i.e., the total contributing area (TCA) map; and (iii) the estimation of the stream network after specifying a threshold value that defines the minimum drainage area required to initiate a channel. In this work, threshold values equal to 0.02, 0.1, and 1 km^2 are used to extract the stream network for basin areas smaller than 1 km^2, basins between 1 and 10 km^2, and basins larger than 10 km^2, respectively.

The catchment boundaries resulting from the delimitation are finally made available in vector format in the WGS84 UTM32 N (EPSG 32632) coordinate system. The catchment boundaries were used as masks to clip several layers of climatological and soil-related attributes. Moreover, the provision of this geographic information will allow users to expand this database by computing other descriptors using possible new gridded datasets.

In this work, we first selected from the literature a large set of morphological attributes that can be directly obtained by processing the 30 m resolution STRM DEM. Automatic procedures based on the GRASS add-ons *r.basin*, *r.stat*, *r.slope.aspect*, *r.stream.stats* (Jasiewicz, 2021) and *r.accumulate* (Cho, 2020) are used for this computation. This leads to 61 geomorphological attributes (see Table 1 of Claps et al., 2024, for a complete description).

3.1.a.1.4 Data and catchment attributes concerning the soil, vegetation and climate

Soil descriptors included in the FOCA dataset can provide information connected to an area-averaged estimate of the soil permeability conditions. These descriptors are the mean areal values of the curve number (Soil Conservation Service, 1972) and of the saturated hydraulic conductivity. The curve number values used in this study were taken from a national-scale cartography produced by Carriero (2004) at 250 m resolution. To derive a feature that approximates soil permeability features, we started from soil texture fraction maps derived from SoilGrids (Hengl et al., 2017; available at https://soilgrids.org/). These cartographies map the spatial distribution of soil properties across the globe at 250 m spatial resolution and at seven standard depths ranging from 0 to 200 cm. Based on the sand and clay contents, we derived the saturated hydraulic conductivity using the pedo-transfer function proposed by Saxton et al. (1986; Eq. 3). The list of soil attributes that we computed is reported in Table 2 of Claps et al. (2024).

Land cover characteristics at 100 m resolution are extracted from the 44 classes of the third level of CORINE Land Cover 2018 (available at https://land.copernicus.eu/). In particular, 5 land indices obtained by merging similar classes are considered here. We also computed multi-temporal indicators of the NDVI (Normalized Difference Vegetation Index) maps, whose data are provided by the Copernicus Land Monitoring Service

(available at https://land.copernicus.eu/). The NDVI is an index that shows whether the area under investigation contains live green vegetation and shows its overall health. We used the values of the Long Term Statistics (LTS) NDVI V3.0.1 of the Copernicus service (with a 1 km spatial resolution), which are mean NDVI observations over the period 1999–2019 for each of the 36 periods of 10 days per year, resulting in 36 raster maps. These maps were used to compute the mean NDVI value, the (temporal) coefficient of variation of the NDVI, and the spatio-temporal mean NDVI regime. The NDVI regime is a graphical representation of the multi-temporal mean calculated over 36 time intervals, each spanning 10 d. To synthetically characterize the latter, a Fourier series representation was used, which allows the shape of the regime to be described with fewer parameters (four in total) than the 36 average values (each for a different 10 d period) from which it is composed. A more detailed description of the four parameters that describe the coefficients of the Fourier series that represent the NDVI regime is reported in Appendix A of Claps et al. (2024). After this data preparation, catchment boundaries were used to extract a total of 11 land cover and NDVI attributes, as listed in Table 3 of Claps et al. (2024).

Mean monthly precipitation information is taken from the BIGBANG (Bilancio Idrologico GIS BAsed a scala Nazionale su Griglia regolare; Braca et al., 2021) 4.0 dataset, which covers the 1951–2019 period. BIGBANG is obtained by means of the spatial interpolation of rain gauge measurements at 1 km resolution, and integrates, only over limited areas and for certain years, the spatial interpolation produced by ARCIS (Archivio Climatologico per l'Italia Centro Settentrionale). Mean monthly temperature data are also derived from this dataset. Both mean monthly precipitation depths and mean monthly temperature data are processed to compute the mean coefficients of the Fourier series that approximate the precipitation and temperature regimes (four coefficients for rainfall and four for temperature; see Appendix A of Claps et al. (2024)). This dataset is also used to compute the mean annual precipitation (MAP) and the mean annual temperature (MAT). Catchment boundaries were used to clip the abovementioned precipitation and temperature maps and obtain spatial averages for the 14 climatological attributes listed in Table 4 of Claps et al. (2024).

3.1.a.1.5 Extreme rainfall catchment attributes

With respect to other national databases, one of the main novelties of this work is the introduction of information related to parameters of the sub-daily precipitation extremes. This inclusion was made possible thanks to the availability of a rich collection of in situ data that is characterized by a much greater accuracy when capturing extremes compared to reanalysis data like the ERA5 and ERA5-Land datasets widely used in the creation of other datasets. The annual maximum rainfall depths used to derive spatial extreme rainfall statistics are obtained from the Improved Italian – Rainfall Extreme Dataset (I^2-RED; Mazzoglio et al., 2020). This dataset consists of official and quality-controlled short-duration (1, 3, 6, 12, and 24 h) annual maximum rainfall depths recorded by more than 5200 rain gauges across Italy between 1916 and 2019.

This FOCA dataset represents the first national-scale collection of mean extreme rainfall catchment attributes. Rainfall data and related statistics are processed at 250 m resolution with the R function *autokrige* (Hiemstra and Skoien, 2023). This performs automatic ordinary kriging using the variogram that best fits the data, which is automatically generated by the R function *autofitVariogram*. The rainfall statistics obtained with this procedure are the scale factor a and the scaling exponent n of the average intensity–duration (ID) curves, which are obtained by linear regression of the logarithm of the average rainfall depth h_d for the durations of 1 to 24 h against the logarithm of the duration, the coefficient of L-variation (*L-CV*) for the durations of 1 to 24 h and the coefficient of L-skewness (*L-CA*) for the durations of 1 to 24 h.

3.1.a.1.6 Peak and daily discharge collections

The peak and daily discharges from each gauging station come from Claps et al. (2020a, 2020b, 2020c), which is the most up to date systematic flood collection in Italy. Until the 1970s, the data reflect most of the content of *Pubblicazione no. 17* of the SIMN. After that, a consistent integration was carried out by merging data from different sources.

3.1.a.2 Flood response time in ungauged basins

3.1.a.2.1 Introduction

In the last decades, runoff prediction in ungauged basins (PUB) has received great attention from hydrologists and several methods for predicting basin response are currently available. Where no in-situ runoff data exist, rainfall-runoff transformation models have traditionally been employed. Many of these models are based on the concept of the basin response function (Sherman, 1932), which can be adopted to obtain discharges at the basin outlet produced by any given excess design rainfall through convolution. One of the key parameters that may be needed to specify the response function is the characteristic time of the basin hydrological response.

For design purposes in ungauged basins, empirical or analytical formulas are typically adopted to compute the characteristic time of the IUH function. A huge number of formulas is available in the literature: the works by Carter (1961), Chow (1962), Kirpich (1940), McCuen et al. (1984), and Soil Conservation Service (1972) are among the most cited. Some of these formulas, more than others, have become popular over the years. However, this popularity does not always correspond to estimates whose uncertainty is clearly understood. At the same time, because multiple definitions for response time, each based on differing assumptions, have been coined over the years, formulas have been often misused. Furthermore, in the engineering practice, the use of one or more formulas is often justified on heuristic grounds, lacking solid scientific considerations to guide the choice towards the most appropriate formulation.

An effort to address the fragmentation problem outlined above is essential, in order to identify a limited pool of formulas providing hydraulically consistent and robust results to be used in the prediction step of the hydrological modelling.

3.1.a.2.2 Formulas for the estimation of characteristic response times

As mentioned in the previous section, when estimating the hydrograph time parameters in ungauged basins the user has to choose from a large set of available relationships and must face some difficulties in their practical use. These challenges arise from existing differences in parameter definitions, differences in units, and the limited regional applicability of empirical formulas, as pointed out by Sheridan (1994).

With the aim of proposing a methodological approach to provide support in choosing a robust formulation for estimating basin flood response time, 29 formulas have been carefully selected from the literature. All the formulas contain parameters related to the basin's length and slope. After verifying the real meaning of the input parameters and units required by the formulations in the original articles where they were published, the structure of the formulas considered has been analyzed in dimensional terms, using a reasoning scheme consistent with the hydraulic relations of resistance formulas, like Chezy's or Manning's. Formulas using a single parameter (area or length) are compared with others that include both, demonstrating how many empirical formulas approximate a theoretical relationship between the exponents of length and slope, specifically a 2:1 ratio. Formulas that are consistent to this ratio are referred to as "hydraulically consistent," and a total of 13 such formulas have been identified.

3.1.a.2.3 Assessment of the robustness of formulas

In order to identify which formulas are more robust, the average streamflow velocities provided by each of them have been computed over 135 basins in north-western Italy. The average velocity is used here as a more meaningful parameter for comparisons than travel time. Travel times cannot easily be compared with reference values because their scaling with lengths and basin areas is quite undefined. In other words, it is difficult to identify the “object” for which we measure travel time and its “true” value cannot be directly measured or determined (Sharifi and Hosseini, 2011). This uncertainty can be partially solved when relying on the inferred velocity estimates that each formula provides.

Starting from the celerities obtained as the ratio between the length of the basin's drainage path and the response times provided by each formula and using the morphology of the river network of the above-mentioned 135 catchments, the variability of estimated mean travel velocities is assessed. To ensure comparability,

time parameters have been standardized, with widely accepted conversion factors applied, such as a factor of 1.67 to convert a lag time into a time of concentration.

A first question to address is how reasonable, i.e. consistent with observations, the velocity estimates obtained are. Literature observations, such as those by Leopold (1953), suggest that stream velocities typically range between 0.5 and 3 m/s during flood flows, with outliers occasionally exceeding this range. The second and even more relevant aspect is to check which velocity behavior (i.e. increasing, decreasing or even constant) as a function of the catchment size, would be the most appropriate. The hydraulic geometry studies led by Leopold and Maddock (1953), contrary to the impression that upstream velocities are higher due to steeper slopes, reveal that average velocities increase downstream. This is due to greater depths downstream, which compensate for the reduction in slope, as described by the Manning equation. Similar evidence has been observed by Pilgrim (1977), Jowett (1998), and Shook et al. (2024), with velocities increasing slightly with watershed size.

Therefore, an increasing pattern with basin size is accepted, while decreasing velocities are considered to be not consistent with observations. A separate discussion should be made for small basins, which are characterized by steep slopes on the one hand, and a hydrological response mainly governed by hillslope flow, on the other hand. Velocities produced over small basins (i.e. over basin areas smaller than 30 km^2, for which no observations are available) should be therefore approached with caution. For safety reasons, it is reasonable to assume that velocities in small basins might remain relatively constant.

3.1.b Enhanced methodologies of flood assessment over network legs

3.1.b.1 Guidelines on the evaluation of the flood-related hazard

3.1.b.1.1 Introduction

Extreme weather events, particularly floods, severely disrupt transportation infrastructures, leading to significant economic and social consequences (Bíl et al., 2015; Dong et al., 2020). Floods directly impact roads and railways by submerging routes, causing delays, rerouting, or cancellations of services, and triggering cascading disruptions to energy and urban systems (Pant et al., 2018). Climate change exacerbates these challenges, increasing the frequency and severity of such events (Wang et al., 2020). Assessing flood risks to transport networks involves major challenges, including the large-scale impacts of river floods, infrastructure complexity, and limited high-resolution hazard data (Prudhomme and Genevier, 2011; Chang et al., 2010). System-level approaches, such as those using OpenStreetMap and global hazard maps, estimate that 7.5% of global transport assets face a 1/100-year flood risk (Koks et al., 2021). Advanced techniques like fragility functions and machine learning enhance risk understanding (Tsubaki et al., 2016).

In Italy, 24% of the 16,787 km railway network is exposed to flooding and erosion, with significant vulnerabilities in urban floodplains and hilly regions (Firmi et al., 2021). However, comprehensive hazard mapping remains incomplete, limiting precise risk assessments (Samela et al., 2023). Key aspects include: i) high spatial resolution, focusing on individual segments of the infrastructure network; ii) characterization of flood impacts, detailing the type and severity of potential hazards for each segment, such as damage from embankment overtopping, instability due to erosion or infiltration, vehicle collisions with debris or flood deposits, and other specific flood-related risks; iii) flood hazard classification, prioritizing intervention actions based on the severity of risks; iv) comprehensive hazard assessment, which integrates existing, state-of-the-art fluvial and pluvial hazard maps alongside methods to assess risks across entire river networks and on hillslopes outside the river network, for fluvial and pluvial flooding, respectively. These methods enable large-scale applications, fostering effective risk mitigation and resilience strategies. By preparing targeted network management plans, stakeholders can proactively minimize the adverse impacts of natural hazards, ensuring a robust and adaptable transportation infrastructure.

3.1.b.1.2 Method

The identification of at-risk infrastructures and the classification of flood phenomena threatening them follows a structured approach, enhancing the ability to identify vulnerabilities and improve resilience. The methodological framework involves three key steps (Samela et al., 2023):

- identification of vulnerable infrastructure segments. This step involves pinpointing sections of land transport networks that may be affected by water-related hazards, using official hazard maps or other data sources.
- characterization of hazardous events. Based on a few geomorphic parameters, such as slope, watershed concentration time, and potential debris flow sources, this step involves estimating the flood-related hazards by analyzing the topography of the basin, typically derived from a Digital Elevation Model (DEM).
- damage scenario identification and hazard classification. This final step links the previously estimated parameters to specific damage scenarios and assigns a flood hazard class to each infrastructure segment, enabling prioritization and targeted risk mitigation strategies.

In this context, this document contains specific guidelines in terms of: i) selection of input data; ii) user-friendly elaborations (to be carried out with any GIS software); iii) Flood Risk Classification, related to both physical assets of infrastructures and traffic management.

3.1.b.1.2.1 Identification of vulnerable infrastructure segments

The European Floods Directive (2007/60/EC) requires River Basin Authorities to map flood-prone areas under three scenarios: H1 (rare events, return period up to 500 years), H2 (frequent events, return period 100–200 years), and H3 (very frequent events, return period 20–50 years). These flood hazard maps are integrated into Flood Risk Management Plans (FRMPs), which are updated every six years to maintain accuracy (Samela et al., 2023). In Italy, the 2021 dataset provides extensive coverage, though smaller streams are often omitted. Infrastructure sections (RSs) exposed to floods are assessed for multiple hazard levels, with H3 areas also at risk from H2 and H1. Each scenario requires separate evaluations of hydraulic parameters, like water depth, to ensure a thorough risk assessment of all transport infrastructures, including rail and road networks (Bíl et al., 2015; Dong et al., 2020).

3.1.b.1.2.2 Characterization of hazardous areas

In flood hazard areas, reference points are used to mark locations for geomorphological and hydrological analysis of land transport infrastructure. When infrastructure intersects with the river network, reference points are placed at these intersections. If the infrastructure passes through flood-prone areas without directly crossing the river, the reference point is determined by the closest river point along the steepest descending path from the infrastructure's downstream end. This approach ensures consistent reference points for assessing flood risks across different transport networks, such as roads and railways (Serre and Heinzlef, 2018).

3.1.b.1.2.2.1 Potential debris flows sources

The flood hazard scenario involving debris flow impacts on land transport infrastructure arises from the proximity of potential debris flow source areas, which could threaten infrastructure integrity. Debris flows typically occur due to intense rainfall on steep slopes with sediment. Mapping these areas is crucial for identifying at-risk infrastructure. Methods to identify debris flow source areas often rely on morphological and topographical parameters, such as slope and upslope contributing areas, which can be derived from Digital Elevation Models (DEMs) and geological maps. Debris flows are likely in areas with more than 10 hectares of contributing area and slopes over 27%. A slope threshold of 78% is considered the point beyond which debris flows are unlikely. However, proximity to a source area doesn't guarantee that infrastructure, like railways, will be affected, as debris flows typically travel up to 500 meters. A safety margin of 1 km is applied to assess risk, with sources within 1 km considered a risk and those farther away disregarded (Pastorello et al., 2017; Fannin and Wise, 2021; Samela et al., 2023).

3.1.b.1.2.3. Damage scenario identification and hazard classification

The final step involves assessing the exposure of each land transport infrastructure section to potential damage scenarios (e.g., overtopping, infiltration, washout, or impact from alluvial materials) and assigning a corresponding flood hazard class.

3.1.b.1.2.4. Proposed technical guidelines

To implement the proposed technical guidelines, both the identification of essential input data and the execution of GIS-based analyses are key steps. These processes form the foundation for understanding flood risk and its potential impact on infrastructure.

3.1.b.1.2.4.1 Input Data and Procedure

Primary level (mandatory data)

- Shapefiles
  - Railway network, distinguishing between high-speed and traditional paths.
  - Road network, distinguishing between motorways, trunk roads and other (e.g., regional, provincial and municipal) roads.

  - River network.
  - Flood Hazard Maps (FHMs), related to H1, H2 and H3 hazard levels.
- Raster data
  - Digital Terrain Model (DTM), with a spatial resolution of 20-50 m, aimed at hydrologic evaluations (e.g., flow accumulations, time concentration). Higher resolution (1-2 m) DTMs could contain systematic errors such as artificial ridges or valleys because of their method of compilation and the lack of error checking. Consequently, these systematic errors may be interpreted as false channels or obstructions when deriving stream networks in flatter terrain and should therefore be removed prior to stream network prediction.
  - Digital Terrain Model (DTM) or Digital Surface Model (DSM), with a spatial resolution of 1-2 m, aimed at assigning a specific water depth to the road/railway segment of interest.

Advanced level (not mandatory for a basic analysis, but useful data for better specifying the flood risk scenarios)

- Shapefiles
  - Embankments.
  - Bridges.
  - Tunnels.
- Raster Data
  - Outputs from hydrodynamic simulations, in terms of maximum values (for each pixel) for water depth h, velocity v and product $h \times v$.

3.1.b.1.2.4.2 GIS elaborations

In the following we list the primary level analysis.

1. Intersection of Flood Hazard Maps (FHMs) with transport networks.
   To select infrastructure within FHMs that may experience structural damage or traffic management issues, identify affected railway and road polylines by intersecting:
   - FHMs with railway network shapefiles
   - FHMs with road network shapefiles
2. Buffer analysis for nearby affected infrastructure.
   Identify railway and road polylines that, while outside FHMs, could still be impacted by traffic management issues by intersecting:
   - 10-meter buffer of FHMs with railway network shapefiles
   - 10-meter buffer of FHMs with road network shapefiles
3. Segmentation of selected rail/road polylines by dividing each identified polyline into homogeneous segments of 1 to 5 km, considering:
   - Sudden changes in path curvature
   - Significant variations in distance from the river network
4. Reference River Point (RRP) localization for each segment based on:
   - The intersection point between the river network and the rail/road segment
   - If no intersection exists, the nearest river point along the steepest descent path from the downstream end of the segment
5. Terrain Analysis Using GIS (TAUDEM Framework), applying the following routines to a 20-50 m Digital Elevation Model (DEM), whereby each routine generates a raster layer as output:
   - Depitting
   - Flow Direction
   - Slope
   - Flow Accumulation
6. Extraction of key terrain metrics at each RRP at each pixel:
   - Slope (from the Slope layer)
   - Contributing Area (from the Flow Accumulation layer)

3.1.b.1.2.4.3 Flood Risk classification

The Linear Transportation Infrastructure (LTI) segment is assigned a Flood Hazard Class (FHC), which could range from Low (minimal flood risk) to High (significant flood risk with potential disruptions and damages).

3.1.b.1.3 Focus on the infrastructure cross-section: embankment

To maintain embankment effectiveness, safety standards must be followed, including overflow capacity, freeboard height, crest adjustments, and protection against scouring. Railway embankments, though similar to road embankments, face unique risks from floods. These include ballast scour, embankment fill scour, and piping or seepage failure. Ballast scour is the most common issue, and while ballast repairs are easy, damage to embankment fill is more costly. Fragility curves are developed to assess vulnerability (Tsubaki et al., 2016). Upstream flood water levels are used as indicators for railway overtopping failure, as they correlate with the overtopping discharge and influence flow dynamics on the embankment, which are sensitive to variations in crest height and shape (Chow, 1959; Dawson et al., 2005; Apel et al., 2009; Tsubaki and Kawahara, 2013).

3.1.b.1.3.1 Identification of critical sections for track bed overtopping

The identification of critical sections in railway tracks involves analyzing their geometric characteristics and evaluating hydraulic and geotechnical parameters. This helps pinpoint areas vulnerable to overtopping, infiltration, washout, and alluvial material impacts. Among these risks, track bed overtopping is particularly critical, as it can severely disrupt railway operations (Samela et al., 2023). The railway overtopping is critical when:

$$\Delta h = h_{pf} - h_w < 2.5\ m \tag{3.1.1}$$

where Δh is the freeboard, h_{pf} is the height of the rail and h_w is the water depth.

3.1.b.1.3.2 Fragility curves for railway embankment and ballast scour

The properties of ballast, embankment fill, and surface cover in railway embankments are standardized but still exhibit variability, particularly in aging infrastructure, leading to high uncertainties in material properties. This issue mirrors challenges in river embankment overtopping, where probabilistic approaches are used to handle uncertainties (Dawson et al., 2005; Apel et al., 2009). To assess damage probability, a fragility curve approach is employed, often using a two-parameter normal distribution or log-normal distribution function (Shinozuka et al., 2000; Suppasri et al., 2012; Mas et al., 2012). This probabilistic framework provides a more reliable evaluation of failure likelihood under varying conditions. The significant uncertainties in embankment properties make deterministic evaluations less effective, necessitating the use of probabilistic methods for accurate risk assessment (Dawson et al., 2005; Apel et al., 2009). The assessment of the two model parameters (i.e. median and standard deviation) is performed by maximizing the likelihood function. For binary damage outcomes (damage or no damage), the likelihood function is expressed as

$$L = \prod_{i=1}^{N} [P(a_i)]^{x_i} [1 - P(a_i)]^{1-x_i} \tag{3.1.2}$$

where

- a_i is the hazard level (overtopping water depth in this study) of sample number i;
- x_i = 1 or 0 indicates embankment scour or no breach, respectively, under the corresponding damage type;
- N is the total number of samples.

The assessment of the river and floodplain flows can be calculated by using a hydraulic model or by solving the shallow water equations (Tsubaki and Kawahara, 2013).

3.1.b.1.3.3 Instability due to flooding and seepage

The risk of failure in transportation embankments due to seepage is well-recognized, particularly for dam embankments, but is also significant for railway and road embankments. This risk is influenced by three main factors: flooding events, hydraulic weaknesses, and geotechnical weaknesses (Polemio and Lollino, 2011). Seepage from upstream hydraulic heads can lead to embankment failure, especially in transportation embankments at critical drainage points, where the risk is linked to temporary upstream impoundments caused by flood events and hydraulic weaknesses (Japanese Geotechnical Society, 2006). Flood events, including peak discharges and secondary floods, along with hydraulic weaknesses like obstructed drains or under-designed infrastructure, contribute to seepage-induced failures, which may result in slope sliding or internal erosion. These failures can lead to embankment collapse. Internal erosion manifests in three forms: backward erosion, suffusion, and concentrated leakage erosion, all potentially leading to breach formation through the enlargement of erosion pipes, downstream slope instability, or overtopping due to crest settlement (Fell et al., 2003; Wan and Fell, 2008). Risk assessment should focus on the entire transportation network, though it is more feasible at the watershed scale, involving three stages: historical flood damage analysis, peak impoundment assessment, and embankment stability analysis. These stages include examining past flood events, quantifying peak floods at embankments, and evaluating embankment stability using geotechnical methods and techniques to assess risks such as internal erosion (Terzaghi, 1939; Lane, 1934; Wan and Fell, 2008). This comprehensive approach enables effective risk assessments for embankments (Polemio and Lollino, 2011).

3.1.b.1.4 Focus on the infrastructure cross-section: bridges

To assess the vulnerability of road bridges during floods, factors such as vehicle stability in submerged conditions, flood characteristics, flood occurrence probabilities, exposure to floods, and bridge susceptibility to damage must be considered (Buonora et al., 2024). This evaluation identifies instability risks for vehicles crossing fords, vented fords, and bridges. The potential catastrophic consequences of bridge hydraulic failure make vulnerability assessment a primary concern for authorities (Brath and Montanari, 2000). Primary bridge damage due to floods includes: i) subsidence of piers due to foundation erosion; ii) damage or destruction of the deck; iii) total collapse of the platform. These damages are mainly caused by water pressure, erosion, impact from boulders or logs, and channel instability (Gschnitzer et al. 2017).

3.1.b.1.4.1 Erosion at the bridge' piers and abutments

Erosion is a common cause of bridge damage, primarily due to river currents that mobilize and transport riverbed sediments. General erosion occurs when the bridge structure reduces the riverbed's cross-sectional area, accelerating the current and causing erosion. Various formulas, including one by Straub (1934), are used to assess the depth of generalized erosion, with many similar to his original formulation.

$$\frac{h_r}{h_m} = \left(\frac{B}{b}\right)^{6/7} \left[\frac{\tau_e}{2\tau_m} + \sqrt{\left(\frac{\tau_e}{2\tau_m}\right)^2 + \left(1 - \frac{\tau_e}{\tau_m}\right)\frac{B}{b}}\right]^{-3/7} \quad (3.1.3)$$

where:

- h_r, and h_m, are the water heights, respectively, in the undisturbed section and in the narrow one;
- τ_e is the mean tangential action exerted by the current on the riverbed in conditions of incipient motion of the riverbed material;
- τ_m, is the same tangential action in correspondence of the indi-unclimbed section;
- B and b are the widths of the water surface in the riverbed sections, respectively, indi-unclimbed and restricted.

Localized erosions occurring at the base of the bridge's piers or abutments are the most frequent causes of bridge collapse or damage. When a flood occurs, the water velocity rapidly increases from upstream to downstream, bringing the downflow water from the water surface to the bottom around the bridge piers.

The main factors influencing the erosion process at the base of the piers are the speed and depth of current, the width of the pier and its shape, the length of the pier and the angle of attack of the current, the nature of the riverbed material and any debris carried by the current. The extent of erosion also depends closely on the solid transport of the watercourse. The estimate of the maximum depth potentially reached by the excavation is made complex by the cyclical nature of the phenomenon. The excavations, in fact, generally reach the greatest depths during the alluvial events, in particular at the moment of the transit of the peak of flow, and then be partially or totally filled in the phase of exhaustion of the hydrogram of flood. The erosion at the base of bridge stacks can be estimated the following relationship:

$$e_r = 2k_p k_\Theta k_c \left(\frac{a}{h_m}\right)^{0.65} h_m F_m^{0.43} \quad (3.1.4)$$

in which:

- a is the width of the pile;
- h_m, and F_m, are respectively the water tie and the Froude number of the current immediately upstream of the pile itself;
- k_p, k_J, k_θ and k_c are corrective factors that consider, respectively, the geometry of the batteries, the shape of the riverbed, the angle of incidence of the current and the effect of any armoring.

3.1.b.1.4.2 Expeditious assessment of the hydraulic vulnerability of bridges

The expeditious assessment procedures described are aimed at the rapid identification of crossings subject to greater risk and their main causes of vulnerability, in order to identify a scale of priority of the necessary actions in order to secure the existing river crossings within a certain geographical region.

In the following, there is a brief analysis of international procedures for rapid assessment of the vulnerability to erosion of river crossings. According to a method developed by Hydraulic Research Ltd commissioned by the British Railway Board, the degree of vulnerability to erosion of the riverbed foundations of the bridge is estimated through an overall *RN* vulnerability indicator, expressed as

$$RN = PPE + TR - FQ \quad (3.1.5)$$

where *PPE*, *TR* and *FQ* are three independent factors that identify, respectively, the potential predisposition to the erosion of the riverbed, the general conditions of stability of the watercourse and banks, and, finally the vulnerability of the foundations of the structures in the riverbed of the bridge (Brath and Montanari, 2000).

3.1.b.1.4 Focus on the infrastructure cross-section: tunnels

The risk of tunnel flooding is a critical concern in the evaluation and management of highway and urban tunnels (Wu, 2020). With the potential for frequent occurrence of traffic accidents and the impact on the safety of people's lives, property, and nearby buildings, it is crucial to implement effective measures to mitigate this risk (Tian et al., 2020). During heavy rainfall and flooding, water can overwhelm drainage systems, leading to excessive accumulation within the tunnel and posing risks to infrastructure integrity and transportation safety (Siregar et al., 2020). Tunnels are probably the most vulnerable parts during an underground flood event. Floodwater could burst into subway tunnels from different places, such as platforms of the station, exposed railway depots, and some broken points on pipelines or waterproof structures (Dong et al., 2024).

In particular, the main causes of water hazards in tunnels can be distinguished into internal factors, associated with the hydrogeological conditions in which the tunnel was built, and in external factors, associated with extreme weather conditions such as floods or heavy rainfall (Ma et al., 2022).

1. The tunnel construction induced ground cracks have been identified as a significant issue. These ground cracks have resulted in the infiltration of surface water, compromising the surrounding loess and leading to heightened loads on the tunnel structure. This has ultimately resulted in extensive

cracking of the tunnel lining, posing serious threats to the safety and durability of the tunnel (Lai et al., 2017).

2. Collapse of tunnel entrances under rainfall conditions can be a particularly concerning issue, as it poses threats to both the stability of the tunnel structure and the safety of surrounding areas. The collapse mechanism of tunnel entrances under rainfall conditions is often attributed to the reduction in soil shear strength caused by an increase in soil water content. In fact, water from precipitation or flooding, can infiltrate the surrounding rock at the entrance of the tunnel can lead to erosion and softening of the material, which are the main causes of tunnel collapse (Chen et al., 2022; Yang et al., 2018).
   In particular, it has been shown that the mechanism of the decrease in soil shear resistance caused by the increase in water content can be explained by the change in matrix aspiration between soil particles. Indeed, the change in soil moisture content is closely related to soil stability and is a cause of numerous landslides (Lin et al., 1936). The reason is that when the soil changes from unsaturated to saturated state, the aspiration of the matrix between the soil particles gradually decreases to 0 (Chen et al., 2022). Before the rainfall, the soil on the entrance slope of the tunnel was in an unsaturated state with low water content, and all meniscus between soil particles were independent of each other. Because the plastic deformation of soil is interpreted as sliding between soil particles, the matrix suction resisted the plastic deformation of soil when the soil water content was low. At this water content, the entrance slope was in a good state of stability. When the rainfall started, the water content of the soil mass of the entrance slope gradually increased from the tunnel to the surface (Mahmood et al., 2018). The matrix suction between soil particles also decreased gradually from the tunnel to the surface. Therefore, the shear strength of soil presented the change law of decreasing from the tunnel to the surface. At this time, the soil can be roughly divided into saturated soil and unsaturated soil along the vertical direction. Due to the increasing water content of the unsaturated soil, the unsaturated state between soil particles changes. The meniscus in the soil pores was gradually connected. The pressure caused by matrix suction can be transmitted between soil particles, which can cause the compression of soil and reduce the stability of the entrance. When the soil mass in a certain depth below the surface of the tunnel entrance slope reached a saturated state, the matrix suction of the soil mass dropped to 0, and this part of the soil mass was prone to sliding.
3. There are hydraulic tunnels subject to high internal water pressure (HT), which are mostly used to transport water from the tank to the hydropower plant machine building with turbines. The hydraulic fall that exists between the tank and the power plant produces the internal water pressure in the hydraulic tunnel. Internal water pressure can cause tensile stresses and cracks in the concrete tunnel lining and thus generate static instability in terms of failure and functional instability in terms of water leakage from the tunnel. Water loss in the tunnel occurs through various cracks and cracks in the concrete lining (Radovanović et al., 2022).
4. Floodwaters pressure can contribute to erosion and the consequent transport of debris inside the tunnels. Blockages can then occur that hinder the proper functioning of drainage systems (Abegaz et al., 2024).
5. Structures close to the coast are particularly susceptible to flooding. In fact, some of the road tunnels are below sea level and are therefore vulnerable to flooding, and vulnerability could increase with rising sea levels and climate change (Jacobs et al., 2018; Li et al., 2022).

3.1.b.2 Flood scenarios generation at regional scale under current climate conditions

3.1.b.2.1 Introduction

Floods represent a significant threat to communities and infrastructure worldwide. The ability to predict and manage these events is crucial to minimizing their impacts. In this context, the concepts of risk, hazard, and vulnerability are fundamental in flood assessment and management. Risk refers to the probability of a harmful event, such as a flood, occurring and its potential consequences. Hazard is related to the likelihood of such an event happening, while vulnerability refers to the susceptibility of a community or infrastructure to suffer damage due to the flood.

Italy has experienced significant losses due to flood events, with 3182 deaths, 86 people missing, 1904 injured, and more than 690,000 evacuees who lost their homes during the period 1861-2013. Currently, the assessment of hazard and risk is the responsibility of River Basin Authorities and the corresponding regions.

This information has been synthesized by ISPRA for the Ministry of the Environment across the entire country. Hazard is considered in three possible scenarios: high probability (with a return period T = 20-50 years, where T is calculated in terms of non-exceedance probability P, i.e., $T = 1/(1-P)$); medium probability (return period of 100-200 years); and low probability (return period greater than 200 years). The percentage distribution of flood hazard across the territory based on the report provided by ISPRA (2018) is 4.1%, 8.4%, and 10.9%, respectively. The regions of Emilia Romagna, Tuscany, Lombardy, Piedmont, and Veneto correspond to the highest percentages.

As established by the EU Floods Directive in D.Lgs. 49/2010, risk must be expressed in terms of: i) the approximate number of inhabitants potentially affected; ii) strategic infrastructures and structures (motorways, railways, hospitals, schools, etc.); iii) environmental, historical, and cultural values of relevant interest; iv) economic activities; and v) installations related to pollution prevention and control.

As presented by Priest et al. (2007) in the risk mapping scheme, two layers of information are necessary: one is the hazard in terms of Depth-Velocity (DV) of the event, and the second is the level of vulnerability in terms of population or a mitigation factor. Through a decision tree (or a hazard-vulnerability matrix), the combination of these two layers produces a risk estimate. In this process, the estimation of the physical components of floods plays the most relevant role. Various models have been used to carry out this task, including empirical, hydrodynamic, and simplified models, according to Teng et al. (2017). Hydrodynamic models, which generally offer better performance, are preferred for estimating flood extent, depth, and velocity. Some of these models include TUFLOW created by BMT WBM in different dimensions 1D, 2D, and 3D (TUFLOW classic, TUFLOW Classic 2D/TUFLOW GPU /TUFLOW FV, and TUFLOW FV respectively), MIKE created by DHI (MIKE11, MIKE21, and MIKE 3), LISFLOOD-FP with 1D and 1D+2D options (coupled model) developed by the University of Bristol, and HEC-RAS and HEC-RAS 2D by the US Army Corps of Engineers. Although these models provide detailed and accurate information about the flood event, their application is limited in extensive areas due to the detailed information required about the terrain, resulting in high economic costs and time needed for each simulation.

In light of the feasibility limitations of hydrodynamic models, simplified and empirical models offer a promising alternative, requiring significantly less computational effort but sacrificing information and increasing uncertainty. These models do not involve physical process simulation but rely on simplified hydraulic processes or direct observations of events. Notable simplified models include the Flood Modeller Pro 2D FAST solver developed by CH2M Hill (formerly Halcrow Group), GFPLAIN205m, a global high-resolution dataset of Earth's floodplains presented in Nardi et al. (2019), or Geomorphic Flood Index (GFI) presented in Manfreda et al. (2015) and later by Samela et al. (2017). GFI has been applied on a large scale in several countries (Samela et al., 2016, 2017, 2018; Tavares da Costa et al., 2019; Manfreda and Samela, 2019), even improving the delineation of flood-prone areas in coastal river basins (Albertini et al., 2022). Comparative evaluations (Neelz and Pender, 2010, 2013) show that this type of model can produce approximate predictions of final flood distributions, with clear benefits in terms of computational cost compared to hydrodynamic models (up to 1000 times faster as claimed by Flood Modeller Pro 2D Fast Solver). Empirical models, alongside the proliferation of remote sensing observations from satellites and unmanned aerial systems (UAS), have supported dynamic mapping of flood events worldwide, such as the Copernicus Emergency Mapping Service (CEMS) with the Sentinel constellation or MODIS with Aqua and Terra (NASA). Albertini et al. (2022) highlighted the potential of multispectral satellite imagery in delineating flood extents, demonstrating the performance of various spectral indices, including the Normalized Difference Vegetation Index (NDVI), the Normalized Difference Water Index (NDWI), the Normalized Difference Moisture Index (NDMI), the Modified Normalized Difference Water Index (MNDWI), and the Water Ratio Index (WRI) from different satellite imagery sources (i.e., Sentinel-2, Landsat, and MODIS).

The products generated by empirical models have been a relevant source for data-driven models. These models use algorithms such as Machine Learning (ML) and Deep Learning (DL) and have the capability to find relationships in high-dimensional nonlinear systems, achieving high performance in flood hazard modeling with low economic and computational costs. Previous studies (e.g., Bui et al., 2019, 2020; Nachappa et al., 2020; Khosravi et al., 2016, 2018, 2019; Kia et al., 2012; Tehrany et al., 2013, 2014a, 2014b, 2015, 2019) explored the potential of ML and DL using methods like Decision Trees (DT), Ensemble models, Neural Networks (NNs), Artificial Neural Networks (ANNs), Support Vector Machine (SVM), Random Forest (RF), and Logistic Regression (LR). In this context, RF presents excellent performance, outperforming

other models (Chang et al., 2019; Nachappa et al., 2020; Motta et al., 2021; Vafakhah et al., 2020; Zhao et al., 2018). Furthermore, RF model applications have spanned various fields, demonstrating high predictive capacity, such as in medicine, landslide susceptibility, and others (Alexander et al., 2014; Zou et al., 2015; Shi & Horvath, 2006; Rodriguez-Galiano et al., 2012; Dai et al., 2018; Du et al., 2015; Mohammady et al., 2019). RF offers high performance with only a few parameters to optimize, enabling variable importance estimation and algorithms for handling missing values (Oshiro et al., 2012; Tang and Ishwaran, 2017).

3.1.b.2.2 Flood available data

To carry out the flood susceptibility mapping, a flood inventory database composed of a total of 280 events was built considering flood records from different sources over a period from 1926 to 2023. In particular, 33 events were obtained from the Copernicus Emergency Mapping Service (CEMS) (https://emergency.copernicus.eu, Figure 1), 24 events from Basin Authorities (Campania, Calabria, and Lombardia), 3 events from the Italian Space Agency, 106 from the Milan Polytechnic Foundation, 107 from regional geoportals (Liguria, Lombardia, Piemonte, Sardegna, Trentino-Alto Adige, and Veneto Regions), and 7 from Regional Agency for Environmental Protection (Piemonte). Finally, permanently flooded areas extracted from the Global Lakes and Wetlands Database were included.

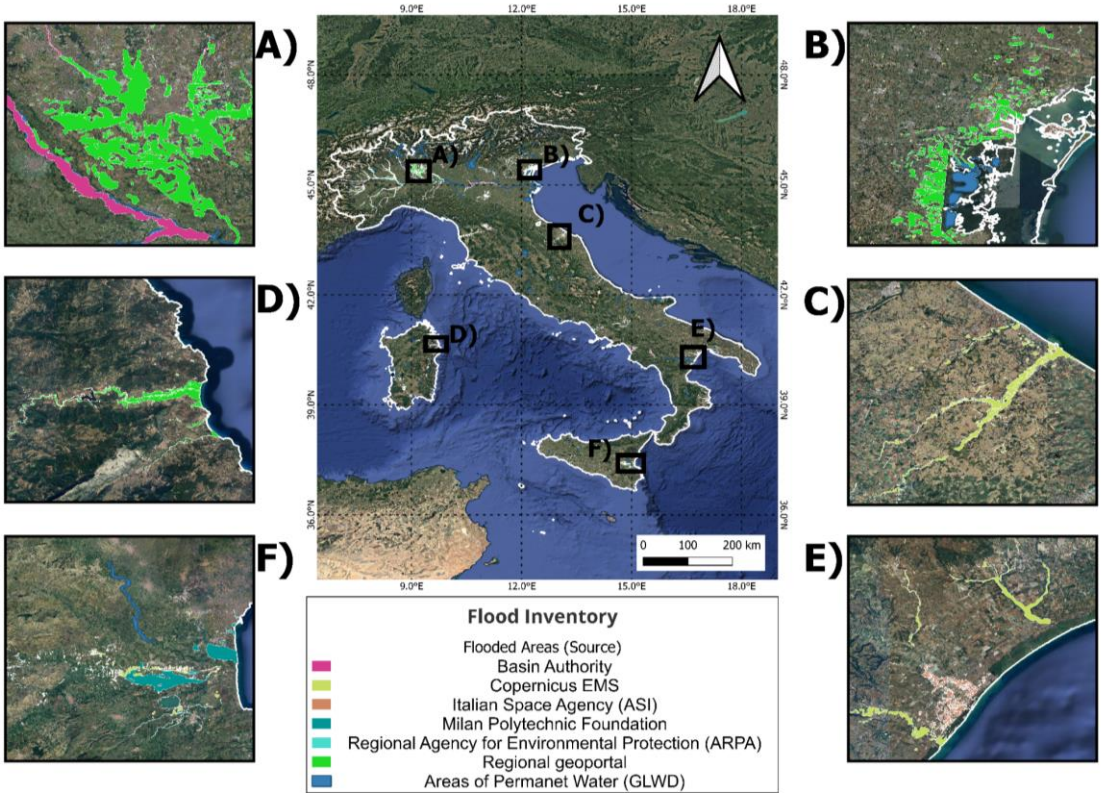

Figure 1. Flood inventory map. Satellite observations and permanent water.

3.1.b.2.3 Methodology and Study Area

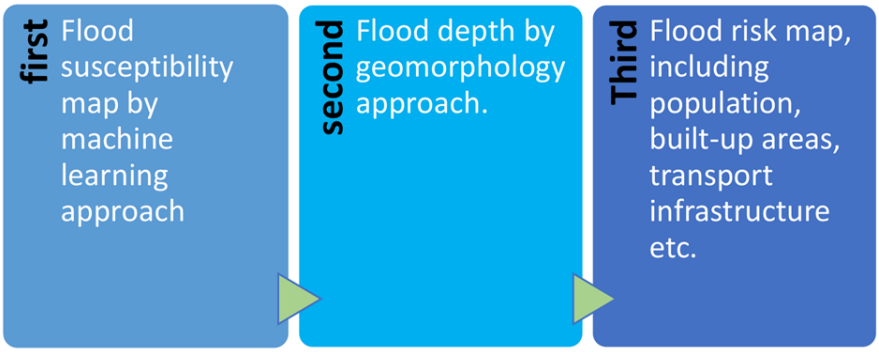

Figure 2. Main components of the flood risk estimation procedure based on geomorphic approach.

3.1.b.2.4.1 Random Forest model and Input Data

Random Forest (RF) is a non-parametric statistical model that employs multiple decision trees combined with the bootstrap aggregating (bagging) approach (Breiman, 1996). This method randomly selects a subset of variables, reducing overfitting effects and improving generalization (Schonlau and Zou, 2020). RF offers high performance with few parameters to optimize, also enabling the estimation of variable importance and the use of algorithms for missing value imputation. Breiman (2001) highlights several advantages of RF:

- High efficiency in large datasets
- Ability to handle a high number of variables without losing efficiency
- Estimation of variable importance using different methods
- Generation of an internal estimate of generalization error (OOB error)
- Relative robustness to outliers and noise (Kulkarni and Lowe, 2016)
- Low computational cost

The applications of the RF model span various fields, demonstrating high predictive capability in medicine, landslide susceptibility, and other areas (Alexander et al. 2014; Zou et al., 2015; Shi and Horvath, 2006; Rodriguez-Galiano et al., 2012; Dai et al., 2018; Du et al. 2015; Mohammady et al, 2019). In flood prediction, it has outperformed ML models, statistical models, and multicriteria decision-making (MCDM) models (Motta et al., 2021; Chang et al., 2019; Vafakhah et al., 2020; Nachappa et al., 2020).

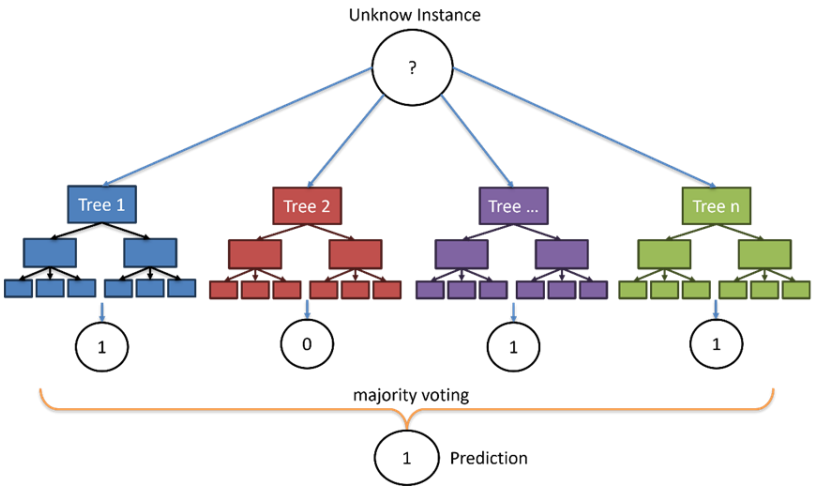

Figure 3. Graphic representation of a random forest classification model.

3.1.b.2.4.2 Analysis of Conditional Factors

The selection of conditioning factors is essential in the creation of flood susceptibility maps using ML models (Wang et al., 2015; Khosravi et al., 2019). In this study, we propose the application of three different methods to estimate the relative importance and their combination to obtain a more representative metric of the information provided by each factor. The Information Gain Ratio (IGR) (Yu et al., 2024), Cohens D index (Cohen, 1988; Rice and Harris, 2005), and ML algorithms has also been applied, demonstrating a high capability to quantify the importance (IQ-RF) (Zhao et al., 2018; Wang et al., 2015; Bui et al., 2020; El-Haddad et al., 2021).

The three methods are combined using a simple average between their standardized values (0 to 1), called Average Merit of Information (AMI). The factors with an AMI value less than 0.3 were removed. Then, in the rest of the factors Pearson correlation and Variance Inflation Factor (VIF) are estimated, the factors with a VIF value greater than 10 and Pearson value greater than 0.7 were removed (Avand et al., 2022).

3.1.b.2.4.3 Evaluation and performance of the model

The evaluation model is based on several key indices to measure the accuracy and effectiveness of classification methods.

Specificity (Equation 3.1.6) assesses the model's ability to correctly identify true negatives, while Sensitivity (Equation 3.1.7) measures its ability to detect true positives. Accuracy (Equation 3.1.8) focuses on the total number of correct predictions made by the model. Additionally, the Kappa index (Equation 3.1.9), along with its components P_c (Equation 3.1.10) and P_{exp} (Equation 3.1.11), provides an adjusted measure of agreement accounting for random chance. Finally, the combined error (Equation 3.1.12) offers a comprehensive view of errors stemming from both false positives and incorrectly identified true negatives.

$$Specificity = \frac{TN}{TN+FP} \quad (3.1.6)$$

$$Sensitivity = \frac{TP}{FN+TP} \quad (3.1.7)$$

$$Accuracy = \frac{TP+TN}{TP+TN+FP+FN} \quad (3.1.8)$$

$$Kappa = \frac{P_c - P_{ex}}{1-P_{ex}} \quad (3.1.9)$$

$$P_c = \frac{TP+TN}{TP+TN+FP+FN} \quad (3.1.10)$$

$$P_{exp} = \frac{(TP+TN)(TP+FP)+(FP+TN)(FN+TN)}{\sqrt{TP+TN+FN+FP}} \quad (3.1.11)$$

$$Combined\ Error = r_{fp} + (1 - r_{tp}) \quad (3.1.12)$$

3.1.b.3 Probabilistic risk assessment for isolated areas in connection to riverine floods under evolving climate conditions

3.1.b.3.1 Introduction and objectives

In this activity, we aim to identify those areas (e.g. small towns) that can remain potentially isolated because of natural events. Particularly, for this activity the focus will be on riverine flooding hazard. The problem is already well recognized and studied in the context of the potential impacts of single events using classical approaches of network analysis (Taylor and Susilawati, 2012; Alasia et al., 2017).

Beyond isolation and remoteness studies, recent works can be found that perform a national-scale analysis of road exposure to flooding by correlating flood hazard maps for different return periods with the road network functionality (Papilloud et al., 2021). Global-scale studies also simulate single events or n-random flood scenarios and use their results to perform the classic percolation method over the road network and analyze functional consequences of flooding (Koks et al., 2023).

However, up to date, we are not aware of studies that address the problem of isolation (that involves road functionality analysis) from a probabilistic point of view. Therefore, our objective is to integrate a road network analysis approach in the framework of a flood probabilistic risk assessment.

The true value of probabilistic risk assessment (PRA) is often misunderstood, primarily because it is perceived as a complex and challenging method to implement and interpret. This complexity can create communication barriers when presenting results. However, a probabilistic risk profile should be viewed as a diagnostic tool, providing critical insights into potential hazards and their consequences.

These profiles encompass all possible risk scenarios within a given geographical area, accounting for both low-frequency, high-impact events and high-frequency, lower-impact events. They quantify the probability of occurrence while incorporating all components of the risk equation—risk = hazard × exposure × vulnerability—along with their variability and associated uncertainties.

Crucially, PRA also considers events that have never been recorded but could arise under future climate projections. This capability is particularly significant as climate change increases uncertainty about hazard patterns. By calculating worst-case scenarios, societies can better prepare for potential impacts. In this context, probabilistic analysis emerges as the only viable method to address such uncertainty in a practical, quantitative manner.

For these reasons, this methodological document presents the formalization of an approach for introducing the evaluation of isolation of remote areas in connection to flood events in the framework of probabilistic risk assessment. In doing this, in the following we will start from summarizing the main characteristics of PRA; then, a possible decomposition of the isolation problem will be introduced, designed for its integration on the PRA framework.

3.1.b.3.2 The Probabilistic Risk Assessment (PRA) framework

In order to perform a scientifically sound probabilistic study it is necessary to produce a set of flood scenarios that result in a collectively exhaustive and mutually exclusive sample. In this context, one should consider that the distinction between flood map and flood scenario is fundamental: flood risk estimates only based on flood maps are reliable if the area of interest is relatively small but, if the area is wide (e.g. country or regional level), it is necessary to generate all possible flood scenarios that can affect the area of interest with their probability of occurrence. Flood hazard maps are pertinent for the overall study area, whereas a flood event or flood scenario usually affects only a portion of the country. The aim of the flood scenarios generation is the simulation of all the possible events that can affect different areas of the region/country with different intensities.

In practice, the simulation process involves dividing the study area into Pertinence Areas (PAs). These PAs are polygons defined at the resolution of the inundation model, establishing a unique correspondence with each stream in the hydrological model's river network. PAs maintain hydrological coherence by associating each segment of the flooded area with the stream of the causative inflow hydrograph responsible for the highest flood depth observed across all hydraulic simulations.

For each PA, the modeled discharge time series is analyzed to identify independent flood events, ensuring an accurate representation of flood scenarios within the probabilistic framework.

For each of the PA, an analysis of the modelled discharge time series is done to select independent flood events.

The methodology that CIMA Foundation uses for the events generation relies on a multivariate statistical approach that takes in input the selected independent events and, by preserving their spatial correlation, it is able to simulate events not yet observed both in terms of intensities as well as geographical distribution. The approach used for the events generation covers all the possible range of intensities and spatial dependencies and assures that:

- the spatial correlation of small- and large-scale events is preserved in the simulated event set;
- the statistical properties of the observed events at each location are preserved in the simulated event set.

The scenario generation process consists of two components: the first one is the event definition and selection, and the second one is the probabilistic events generation. The event selection is based on a consolidated

approach already applied and tested in several countries in Africa (e.g., Rudari et al., 2019; CIMA Research Foundation and Internal Displacement Monitoring Centre, 2024; Trasforini et al., 2024) that balances the need of capturing small scale events and the limited computational resources during the flood generations process. The event selection process is able to identify localized events affecting only one or few PAs and more distributed ones affecting several PA simultaneously.

These events, characterized by their maximum discharge over the event duration for each PA, are the basis for the probabilistic scenarios' generation.

The probabilistic approach applied for the scenarios' generation is based on a probability domain perturbation of the selected flood events via a multivariate gaussian distribution and uses a gaussian transformation in the probability domain to improve the representation of the tail dependencies and overcome boundary issues.

The output of the scenario generation process is a flood event catalogue covering thousands of years.

This event catalogue is then merged with the hazard maps to generate flood inundation maps. Each map is characterized by the water level for the affected cells. These maps are the input data for the risk calculation.

The event set generated with the above-described methodology can be considered representative of current climate conditions if hydrological information is based on reanalysis dataset, otherwise, if different Representative Concentration Pathway (RCP) scenarios are considered, the simulated event set is representative of possible projected climate conditions.

3.1.b.3.3 Classical network analysis literature: discussion on sub-problems

Road networks are a vital component of Critical Infrastructure (CI), serving as a linear system essential for the transportation of goods, people, and services. Recognizing the importance of minimizing damage to CI and reducing disruptions to basic services, international frameworks such as the Sendai Framework for Disaster Risk Reduction, the European Union Commission's infrastructure initiatives, and the COP26 agreements have placed these objectives at the forefront of global agendas.

In analyzing road networks as CI, classical approaches often focus on one or more of the following key elements:

1. Structural Element: this aspect examines the physical state of the road infrastructure, emphasizing damage to bridges, pavements, tunnels, and other physical components. Structural integrity is crucial, as physical damage can render segments of the network unusable, leading to cascading failures in connected systems.
2. Functional Element: this dimension addresses the network's operational performance, particularly disruptions that reduce travel speed, increase travel times, or hinder accessibility.
3. Topological Element: focusing on the connectivity and arrangement of the network, this perspective evaluates how well the road network supports movement between nodes (e.g., cities, intersections) and edges (e.g., road segments). Topological resilience is critical to maintaining accessibility during failures or disruptions.
4. Logical Element: this aspect explores the connections between nodes and edges, emphasizing the relationships and dependencies within the network. Logical analysis often supports understanding of how disruptions in one part of the system might propagate to others, highlighting vulnerabilities and interdependencies.
5. Dynamic Element: reflecting the temporal aspect of road networks, this element examines how the network evolves and changes over time. This includes temporary changes due to construction, long-term changes from urban development, and rapid changes caused by emergencies or disasters.

When analyzing isolated locations, it is essential to assess the road network's capacity to deliver services effectively. This analysis will examine the impacts of each independent hazardous event individually, focusing on the loss of connectivity and functionality. The process involves addressing the following sub-problems:

3.1.b.3.3.1 Identification of potentially isolated locations, based on the road network analysis

The identification of isolated locations using road network analysis involves assessing areas that exhibit limited connectivity and accessibility. The literature presents various approaches to defining and measuring isolation. For example, one method (Taylor et al., 2012) involves creating an index of remoteness for any point on the network with a population exceeding a predefined threshold. This index is calculated as the ratio of the distance from the given point to a specific center and the average distance of all locations to that class of service centers. Another approach calculates remoteness for points on the network derived from the centroids of minimum census subdivisions within a region or country (Alasia et al., 2017). Our analysis aims to pinpoint localities that are intrinsically poorly connected within the road network while hosting a resident population. This involves leveraging network-based metrics and spatial data to identify areas where connectivity gaps exist, potentially hindering access to essential services and broader regional integration. By focusing on population centers with suboptimal connectivity, the study highlights areas where infrastructure or policy interventions may be most impactful.

Let G (N, A) be a direct graph representing the road network, with N the set of nodes I and A the set of oriented arcs (i,j). We define o = 1, …, 0 the node in the network corresponding to a generic potentially isolated location (origin), O being a subset of N.

3.1.b.3.3.2 Identification of centroids representative of service providing locations

Numerous studies have explored road network analysis, particularly its vulnerability to floods and the resulting impact on service provision. A key aspect of such analysis involves determining how local populations might be drawn to other areas or how external populations might be attracted to specific locations. These concepts are quantified using the Population Weighted Index and the Opportunity Weighted Index, as outlined by Wachs and Kumagai (1973), Chen et al. (2015), and Papilloud et al. (2021).

We define d = 1, …, D the node in the network corresponding to the generic service providing location (destination), D being a subset of N.

3.1.b.3.3.3 Identification of optimal paths between pairs of origin and destination nodes

As a first approximation for describing the connection of a couple of nodes origin and destination is to define the shortest path (or minimum cost path) connecting those two nodes in the given network. When trying to understand if a sudden event is blocking the connection between a pair of origin-destination nodes, this assumption could be limitative or provide biased indications. For such a reason, it may be useful to examine not just the optimal solution to a problem but a larger class of solutions, to gain a better understanding of the problem (Eppstein, 1998). In this case we should introduce the k-shortest path problem, for which a generalization of the Dijkstra algorithm (Dijkstra, 1959) can be applied for finding the optimal solution.

The *k-shortest paths problem* is a well-established concept in graph theory and network analysis, focusing on identifying the top k shortest paths between two nodes in a weighted graph. This problem extends the traditional shortest path problem by seeking multiple alternative paths, which is particularly useful in applications requiring redundancy or alternative routing options. This subset represents the most critical routes or pathways that provide essential connectivity within the network, minimizing travel cost or distance across K alternative paths. Connectivity loss in our approach is assessed by identifying disruptions or degradations within these key routes and evaluating their effects on network efficiency, accessibility, and redundancy. The analysis measures how the loss of segments within the K-minimum path affects overall network performance, such as increased travel times, reduced accessibility to vital nodes, or the emergence of isolated sub-networks. This targeted focus allows for a detailed understanding of how disruptions impact the network's most efficient pathways, aiding in the prioritization of maintenance, mitigation strategies, or infrastructure development to preserve or restore critical connectivity.

We define $P_{o,d}^{k}$ as the k-shortest path between the pair of nodes o, d, with k = 1, …, K.

In the following, we will consider the subset of the network composed by the K shortest paths connecting each pair of origin-destination nodes, and we will evaluate direct and indirect effects of an events only on such subset of the original network.

3.1.b.3.3.4 Assessing the Impact of Road Segment Loss on Network Connectivity and Functionality

In the context of probabilistic risk assessment (PRA), direct impacts are typically evaluated using fragility or vulnerability curves/functions. These models are essential components of disaster risk assessments, as they link hazard intensity to the potential extent of damage or loss.

Fragility functions estimate the probability of exceeding predefined damage states (e.g., slight damage, moderate damage, or collapse) for a given level of hazard intensity. These damage states can then be mapped to a corresponding loss ratio or distribution. Vulnerability functions integrate these aspects to directly estimate the average damage or loss ratio associated with specific hazard intensities.

Fragility and vulnerability models can be developed using empirical data, analytical approaches, expert judgment, or hybrid methods that combine multiple techniques. Ideally, these functions should be tailored to the specific exposure characteristics of the region under study, accounting for factors like local construction materials and practices. While empirical data is preferred for its accuracy, it is often limited, especially for rare, high-intensity natural hazard events.

Analytical methods can compensate for data scarcity but rely on simplifying assumptions, requiring a careful balance between model accuracy and computational efficiency. By leveraging region-specific data and adopting appropriate modeling approaches, fragility and vulnerability functions can provide robust insights into potential disaster impacts.

In the assessment of impacts due to floods, the most common approach is to use state-damage functions, or vulnerability functions; in this specific case, the description of the magnitude of the event is usually done by using the maximum water depth associated to the specific element under consideration. Some examples of existing vulnerability curves can be found in literature (see e.g., RED Engineering, 2022, a technical paper which collects some vulnerability models for road elements in connection to floods). A review of existing functions is behind the scope of this paper; nevertheless, we can assume that proper models for the area under analysis can be identified.

We evaluate direct impacts at the level of pertinence areas, identifying with $x = 1, \ldots, X$ the generic pertinence area, we can indicate as $P_{o,d}^{k,x}$ the set of road links belonging to the *k*-shortest path between origin *o* and destination *d*, localized within pertinence area *x*. When considering a specific scenario event, characterized in terms of maximum water depth for each location, we can apply the proper vulnerability function and obtain a further sub-set of links, namely $\left(\bar{P}_{o,d}^{k,x}\right)_e$ the set of road links belonging to the *k*-shortest path between origin *o* and destination *d*, localized within pertinence area *x* and that are non-negligibly damaged by the event *e*. In addition, let's define:

$$\delta_{(i,j)}^{x,e} = \begin{cases} 1 \; if \; (i,j) \in \cup_k \; \cup_{o,d} \left(\bar{P}_{o,d}^{k,x}\right)_e \\ 0 \; otherwise \end{cases} \tag{3.1.13}$$

a Boolean variable assuming value equal to 1 if the arc (*i*,*j*) belonging to set *A* is part of any of the *K* shortest paths between origin *o* and destination *d*, it is localized within the pertinence area *x* and it's non-negligibly damaged by the event *e*.

A synthetic indicator of direct impacts at pertinence area for the generic event e can be defined as:

$$DI_e^x = \sum_{(i,j)\in A} \delta_{(i,j)}^{x,e} \tag{3.1.14}$$

In road network analysis, the impacts of an event are not confined to the footprint of physical damage but extend to broader connectivity disruptions. Therefore, it is crucial to explicitly account for these connectivity impacts using appropriate methodologies and metrics derived from network analysis.

The concept of centrality, initially developed in social sciences, is particular useful in this context; conceptually, centrality measures how central an individual is positioned in a social network (Peng et al., 2018). Several metrics for measuring centrality have been proposed in literature, as for instance betweenness and closeness. Betweenness centrality quantifies the frequency with which a node or edge

falls on the shortest paths connecting other pairs of nodes in the network. Such a metric highlights critical points in the network whose disruption could significantly impact overall connectivity (Freeman, 1977).

Closeness centrality, on the other hand, measures the average distance (in terms of the number of edges or their length) from one node to all other nodes in the network. It provides insights into how efficiently a node can access other parts of the network, emphasizing its role in maintaining overall connectivity. An overview on betweenness and closeness can be found in Bozzo and Franceschet (2013) and Newman (2010).

For each vertex in the network, both betweenness and closeness centrality can be calculated to identify vulnerabilities and critical nodes. This approach helps to assess the cascading effects of disruptions beyond the physical damage area, offering a more comprehensive understanding of the event's impact on the road network. Let's define $c_i \ \forall i \in N$ a value representing betweenness or closeness centrality of node i. A synthetic index representing the loss of connectivity for a generic event e for a pertinence area x can be defined as in the following:

$$CL_e^x = \sum_{(i,j)\in A} \delta_{(i,j)}^{x,e} \cdot c_i \cdot c_j \tag{3.1.15}$$

Assuming that the k paths between each pair of potential origins and destinations are sufficiently representative of the actual connection between the corresponding locations, the non-functionality of one or more of these paths indicates possible isolation. Under the assumption that:

$$\mu_{o,d}^{k,x,e} = \begin{cases} 1 \ if \ P_{o,d}^{k,x} \neq 0 \\ 0 \ otherwise \end{cases} \tag{3.1.16}$$

That is, it takes the value of one only when, within the area x, there are links belonging to the k-shortest path that connects the pair (o,d).

$$\gamma_{o,d}^{k,x,e} = \begin{cases} 1 \ if P_{o,d}^{k,x} \neq 0 \ and \ \left(\bar{P}_{o,d}^{k,x}\right)_e \neq 0 \\ 0 \ otherwise \end{cases} \tag{3.1.17}$$

That is, it takes the value of one only when, within the area x, there are links belonging to the k-shortest path that connects the pair (o,d), and at least one of these links is damaged by the effects of event e within the same area.

The isolation index associated with a generic origin O, as a function of the effects of an event e within the area x, can be defined as:

$$II_o^{x,e} = \begin{cases} \frac{\sum_{k=1}^{k} \sum_{d\in D} \gamma_{o,d}^{k,x,e}}{\sum_{k=1}^{k} \sum_{d\in D} \mu_{o,d}^{k,x,e}} \ if \ \sum_{k=1}^{k} \sum_{d\in D} \mu_{o,d}^{k,x,e} > 0 \\ 0 \ otherwise \end{cases} \tag{3.1.18}$$

If the set of impacted links has a non-empty intersection with $P^k_{(o,d)}$, we can assume that such a path is no longer usable; consequently, the connection between o and d will be reduced, up to the extreme case where none of the k-shortest paths connecting o and d are functional.

The fraction of functional paths serves as an index of potential reachability (indirect impacts).

3.1.b.3.3.5 Inclusion in the probabilistic risk assessment process

The inclusion of this type of network analysis, which is capable of capturing both the direct and indirect impacts of flood events, within a Probabilistic Risk Assessment (PRA) framework offers significant value. This integration enables the estimation of classical risk assessment metrics, including the Annual Average Loss (AAL) and the Probable Maximum Loss (PML).

Specifically, this approach allows for the calculation of the annual average loss of connectivity and functionality at various geographic scales, such as provincial, regional, or national levels. Additionally, it provides a detailed understanding of the losses associated with specific return periods, such as 5, 10, or 25 years. By quantifying these metrics, stakeholders can evaluate the systemic effects of floods on infrastructure networks and identify critical locations that may exacerbate isolation risks.

3.1.c Mapping of coastal flooding induced by extreme wind waves

3.1.c.1. Introduction of methodology

Coastal infrastructure, particularly along low-lying coastlines in Italy, is increasingly vulnerable to flooding from extreme wind-driven waves. These events, already observed today, are projected to worsen with rising sea levels due to global warming. A demonstration study will assess the risk of coastal flooding under various future scenarios, comparing a traditional approach with an innovative method that incorporates future wave projections influenced by climate change. The traditional method uses the ERA5-Reanalysis dataset (Hersbach et al., 2020) alongside direct measurements from the Italian National Wave Network (RON), the National Tide Gauge Network (RMN) (Morucci et al., 2016), and satellite data. In contrast, the innovative approach employs coastal wave climate data from ocean surface wave models, covering the Northwest European Shelf and the Mediterranean Sea, provided by the Copernicus Climate Change Service (C3S) in collaboration with ECMWF, to predict wave behavior under climate change scenarios. A case study will focus on a low-lying coastal area in Tyrrhenian Calabria, where critical infrastructure, such as railways and roads, is highly susceptible to extreme storm waves (Codato et al., 2024).

3.1.c.1.1 Offshore MetOcean data collection

3.1.c.1.1.1. Measurements

Direct measurements made on site are instrumental in type and, if well performed, are generally the best source of information available. The wave buoys and tidal stations provide direct in-situ measurements, serving as a critical reference for calibrating model data. Their role is fundamental in ensuring that numerical models accurately represent the observed wave climate, particularly for extreme events, thereby enhancing the reliability of forecasts and analyses used in coastal management and planning. While satellite data are part of the family of data acquired through indirect measurements performed on site.

As a preliminary step in this analysis, extensive data collection was undertaken, involving wave buoy measurements and requests to the relevant authorities for access to managed datasets. It should be noted that this type of data is not easily accessible to users and, when available, is often only partially so. For this project, some restricted data was formally requested to ensure comprehensive analysis. The meticulous collection and verification of these datasets have also laid a reliable foundation for use by other researchers and practitioners.

A. Historical time series from wave buoys (RON-ISPRA)

The observed wave data are represented by the direct measurements taken by the wave buoys of the National Ondametric Network (RON). It was established in June 1989 under the supervision of the General Directorate of Maritime Works within the Italian Ministry of Public Works and was in function until 2014. The RON is now managed by ISPRA and it represents one of the most accurate and comprehensive oceanographic database for the Mediterranean Sea.

In the past, 14 real-time directional buoys were uniformly distributed along the Italian coastline. Today, not all of those active in the past are still active and nine remain. The history of the network is characterized by two distinct operational phases, each reflecting the evolving approach to data collection and analysis:

- Period I (1989–2002), data acquisition was based on a dual-sampling regime determined by the significant wave height (Hm_0). When wave heights were below approximately 1.5 meters—a threshold set for the Mediterranean Sea—data were recorded at three-hour intervals. However, for wave heights exceeding this threshold, the sampling frequency increased to every 30 minutes. This strategy allowed for a more effective capture of storm events and extreme wave conditions, ensuring critical information was collected during periods of heightened wave activity;

- Period II (2002–2014), the sampling methodology was simplified and standardized. Data were recorded continuously at 30-minute intervals, regardless of wave height. This change provided a more

consistent and detailed monitoring framework, enhancing the ability to track storm events and conduct analyses of extreme wave conditions with greater precision and reliability.

The network's buoys collected synthetic wave parameters:

- Hm_0: Significant wave height, derived from spectral analysis;
- T_p: Peak wave period;
- T_m: Mean wave period;
- Dir: Mean wave direction.

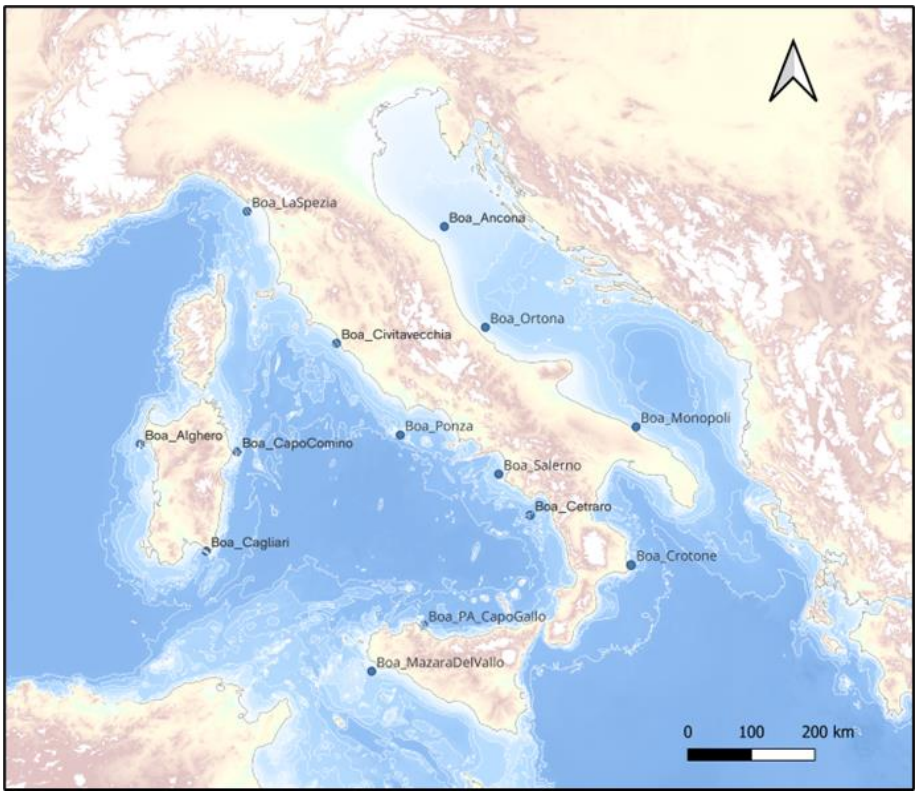

Figure 4 - RON wave buoys in the period 1989-2014.

B. Historical time series from tidal station – sea levels and winds (RMN-ISPRA)

Direct sea level measurements are performed by tidal stations usually located inside harbours or bodies of water that are partially protected from wind-generated waves. Direct wind measurements are performed using anemometers capable of measuring wind intensity and direction.

The mareographic and anemometric data, necessary for the analysis of sea levels and wind, are made up of the observations acquired by the tidal stations belonging to the National Mareographic Network (RMN) managed by ISPRA. The RMN is constituted of 36 measuring stations uniformly distributed over the national territory, which are mainly located within port facilities. At each station, in addition to the tide gauge measured every 10 minutes, the main meteorological parameters of maritime interest such as wind (intensity and wind direction) and atmospheric pressure are also recorded. Wind and meteorological data are always measured in the proximity of airports. Currently, not all stations are operational in real time.

C. Historical time series from wave buoys

In addition to the RON time series, other time series from wave buoys operated by local administrative authorities (e.g. Regions and Port System Authorities) were included. Such as, the Capo Mele buoy (Liguria) managed by Arpal Liguria, the Civitavecchia (Lazio) buoy managed by the Port System Authority and the Cesenatico buoy (NAUSICAA) in Emilia Romagna, managed by Arpae.

D. Historical time series from satellite measurements

Satellite wave data are typically assimilated into reanalysis systems, such as the ERA5 model, to enhance the accuracy of hindcast wave fields. Measurements of the significant wave height from satellite altimeters are integrated to refine the wave model's initial conditions and parameterizations, ensuring better alignment with observed wave dynamics. It is then clear that the possibility of calibrating the hindcasted time series against satellite wave measurements might result in a repetition of the assimilation procedure. It is however well accepted that when comparing satellite and model data in coastal regions a significant bias still exists and it is therefore recommendable to try to further reduce the bias of model data.

In general, the use of satellite measurements for calibration/bias removal of hindcast time series has some points of strength and weaknesses. The point of strength is that worldwide coverage has been guaranteed since 1991, with an increase in time of the number of missions and therefore a larger density of measurements available. The points of weakness are related to the fact that hindcasted data refer to some specific geographical points, while satellites take measurements over their footprint, which typically has a width of several kilometers. Furthermore, satellite data are collected at specific times as the satellite passes over an area, while model outputs refer to specific time levels, e.g. hourly data. One fundamental step that should be undertaken is that of associating the satellite measurements with hindcast data. The proposed procedure is that of associating each satellite measurement with one specific grid point of the hindcast model. Then, one single measurement is extracted for each satellite passage, by taking either i) the one closest to the grid point, or ii) averaging the measures over all the measurement positions related to one specific grid point. Once one single wave height is obtained for each satellite passage, the wave height corresponding to the time of the measurements is obtained by linear interpolation over the time steps of hindcast wave data.

The final result should be a time series of synchronized satellite measurements and hindcast wave data, to be employed for the calibration/bias reduction step.

3.1.c.1.1.2 Model data

A. Historical waves and winds time series from ERA5-Reanalysis (CDS – Copernicus & ECMWF)

The ERA5 dataset, developed as part of the Copernicus Climate Change Service (C3S), represents the fifth generation of ECMWF reanalysis (Hersbach et al., 2020). It is based on the 2016 version of the ECMWF Integrated Forecasting System (IFS) CY41R2 and provides a comprehensive record of the global atmosphere, land surface, and ocean waves. The dataset offers hourly and monthly data spanning from 1940 to the present, archived in the Climate Data Store (CDS). Measurements are carried out using satellites and measurement devices located at sea and on the surface, providing essential data for the reanalysis process in ERA5.

Compared to its predecessor, ERA-Interim (2006), ERA5 features significant improvements. It boasts a much higher spatial resolution of 31 km compared to 80 km, includes uncertainty information, and provides an enhanced number of output parameters such as 100 m wind products. Moreover, it employs 4D-Var ensemble data assimilation, improving the accuracy and reliability of its outputs.

The ocean wave model WAM underpins ERA5's wave simulations. This spectral wave model predicts the growth, decay, and interaction of wind-generated waves. It includes 24 directional bins and 30 frequency bands, accounting for various factors such as wind speed and direction, atmospheric pressure, and sea ice cover, to simulate wave conditions accurately. These features make ERA5 an essential resource for climate studies and long-term analyses of atmospheric and oceanic parameters.

B. Waves and sea levels time series derived from future climate projections (CDS – Copernicus & ECMWF)

Rising sea levels, combined with the increasing intensity and frequency of storm events, are now widely acknowledged as key drivers of heightened coastal flooding risks. This growing threat has profound implications for coastal area management and underscores the need for developing robust, long-term adaptation strategies (Codato et al., 2024; Pasquali et al., 2023; Pörtner et al., 2019). In this context, the

urgency of integrating climate change impact assessments into the management of critical infrastructure becomes clear, emphasizing the importance of implementing preventive and corrective measures to reduce vulnerability and enhance system resilience. To address this, the present study incorporates future wave projection time series, considering potential climate change scenarios. This dataset, provided by the Copernicus Climate Change Service (C3S) in collaboration with ECMWF, offers insights into the wave climate under the influence of climate change for the Northwest European Shelf and the Mediterranean Sea. Projected over a period from 2041 to 2100, the dataset reflects various "Representative Concentration Pathways" (RCPs), each corresponding to different levels of greenhouse gas emissions and their expected impact on future atmospheric conditions. The RCPs, including 2.6, 4.5, 6.0, and 8.5, are linked to radiative forcing (RF) values, which measure the influence of greenhouse gases on the energy balance of the climate system (Meinshausen et al., 2011). In this paper, we focus on the RCP4.5 scenario, which represents a future with moderate emissions and a gradual decrease after mid-century, as well as the RCP8.5 scenario, which projects a future with very high emissions and continued growth, reflecting a pathway without significant climate change mitigation measures.

C. MetOcean Data (VS1-WP4, DICCA - UNIGE)

One of the main datasets provided in Spoke VS1 is the MetOcean database. This data family belongs specifically to the University of Genoa. These data are shared with other spokes implementing some activities on coastal flood risk analysis (such as the TS2 spoke). These data are currently not freely downloadable, but will be shared with the community through the digital twin of VS1. The MeteOcean research group at the University of Genoa has developed high-resolution hindcast datasets and climate change projections. The hindcast dataset (1979-2023) includes two wave models: one with a regular 10-km grid for uniform spatial resolution and another with an unstructured grid for greater detail near the coast, with resolutions down to 300 meters along the Ligurian coast. Both models use WaveWatch III (WW3), driven by wind fields generated by the WRF model, covering the Mediterranean Sea. The datasets include hourly wave parameters such as significant wave height (H_s), peak wave period (T_p) and 2D spectra, validated against in situ buoy and satellite data to ensure accuracy.

The climate change dataset spans from 1970 to 2100 according to the RCP8.5 scenario, using a multi-model ensemble of 21 GCM-RCM Euro-CORDEX combinations. Forced from WW3 with surface wind fields, it provides detailed projections of wave climate with 6-hour temporal resolution and 12.5-km spatial resolution. These datasets support the modeling process for coastal flood risk evaluation.

3.1.c.1.2. Model data calibration - bias correction

Bias correction of model data related to the metocean parameters of interest is of fundamental importance for improving the accuracy of the results. Both hindcast and climate projection models often exhibit discrepancies with respect to real data, due to limitations in physics, resolution, or input data quality. These biases can affect key wave, wind and levels parameters, leading to inaccuracies and systematic errors on the final results. Bias correction techniques range from simple statistical adjustments to advanced machine learning methods, and in general aim at aligning model outputs with observed datasets.

However, model data referring to the past can be directly compared against available measurements for the overlapping time windows. This is clearly not possible for climate projections, that refer to the future and for which direct measurements are not available. The methodology proposed here is that of developing a bias correction method based on the comparison of historical hindcast data and available measurements. The same method is then applied to the climate projections under the assumption that the systematic error of the model chain used to produce the reanalysis data is identical to that of the model producing the climate projections. To this end, it is important to emphasise that the same model used for the CDS - Copernicus & ECMWF climate projections also produced a historical ERA5 dataset (which we will call ERA5-RCP) referring to the years 2001-2017, for which some measurements are available and a direct comparison is possible (Codato et al., 2024).

Bias correction will be performed using the Empirical Quantile Mapping method, ensuring that model data accurately reproduce the statistical properties of the observational dataset (Codato et al., 2024). This approach involves aligning the quantiles of the model outputs with those of the measurements. During the

research it will also be evaluated the possibility of applying some more advanced methods, such as the Parametric Quantile Mapping, that use theoretical statistical distributions (e.g., Gaussian, Gamma).The outcome of the bias correction process will be a calibrated offshore time series, providing the input for the following steps, including wave propagation modeling and the calculation of run-up and flooding.

3.1.c.2 Nearshore Propagation, Run-Up, and Coastal Flooding

3.1.c.2.1. Propagation to Offshore Boundary

The numerical model used for the first phase of large-scale offshore-to-nearshore propagation resolves the spectral inverse refraction of sea states and allows the spectral characteristics of wave propagation from offshore to shore to be determined at a point located on the coast (called the inverse point) using a calculation grid constructed on the basis of bathymetric data of the area of interest. The model reproduces the spatial evolution of sea states represented by a spectrum with energy distributed in frequency and direction, and the effects induced on the wave motion by refraction and shoaling caused by the seabed disregarding dissipative effects due to breaking and bottom friction, thus using a conservative approach. The inversion point was positioned close to the coastline on a natural seabed of approximately 20 meters.

3.1.c.2.2. Large-Scale Propagation to Shoreline

The wave energy spectrum is further propagated toward the coast using high-resolution bathymetric grids, which accurately represent the seabed morphology and its spatial variability. As waves approach shallow waters, several dissipative phenomena come into play, significantly affecting wave transformation and energy distribution. Key processes include bottom friction, wave breaking, and turbulent dissipation.

Bottom friction plays a crucial role, especially in the swash zone, where the interaction between the moving water and the seabed is most intense. The roughness of the seabed, influenced by sediment type, grain size, and bedforms (like ripples and dunes), induces frictional resistance, which extracts energy from the wave system. This dissipation of energy directly impacts the calculation of wave run-up, as it reduces the velocity and height of the uprush. Empirical and semi-empirical formulations will be used to parameterize bottom friction effects, with friction coefficients adjusted to match site-specific sediment conditions.

Wave breaking is another major dissipative process, with energy being lost due to turbulence and air entrainment. As waves break, a portion of their kinetic energy is converted into heat, turbulence, and acoustic energy. This further reduces the energy available for wave run-up.

The final step involves the calculation of wave run-up, which is essential for flood risk analysis and the design of coastal protection systems. The runup parameter will be calculated using analytical formulas as a function of the incident wave parameters at the toe of the beach. Accurate run-up predictions require incorporating the cumulative effects of bottom friction, wave breaking, and turbulence dissipation. The use of high-resolution bathymetric grids ensures that localized seabed features, like sandbars, ridges, or natural slopes, are accounted for. This is critical for spatially distributed wave climate predictions, ensuring that site-specific bathymetric influences are fully captured. Such detailed modeling supports the design of resilient coastal defense systems by providing precise estimates of the maximum uprush, guiding the placement and sizing of coastal protection structures.

3.1.c.2.3.Statistical Analysis of Run-Up Extremes

Statistical analysis of extreme events focuses on identifying the characteristics of phenomena, such as storm waves, that may undergo significant changes under future climate scenarios (Codato et al., 2024). Extreme events are outliers in the data, marked by values that deviate substantially from typical patterns. Extreme value analysis aims to understand the stochastic behavior of processes at extreme levels, focusing on these rare occurrences (Coles et al., 2001).

To conduct a robust analysis, the observed time series must first be verified for statistical representativeness. Extreme values are then extracted using two primary methods rooted in Extreme Value Theory (EVT): the block maxima method and the threshold model. The choice of method depends on ensuring the statistical independence and homogeneity of the data sample. Once extracted, extreme values are analyzed to

determine the best fit between the observed data and theoretical probabilistic models. This enables the estimation of return levels, which correlate synthetic wave parameters to specific return periods or exceedance probabilities. For example, in hydrology, the return period represents the average interval between events of a given magnitude, indicating the likelihood of surpassing a particular threshold (Volpi, 2019).

Extreme value statistics can be derived by sampling annual maxima and fitting a Generalized Extreme Value (GEV) distribution, or by using the Peaks Over Threshold (POT) approach to fit the Generalized Pareto Distribution (GPD).

Although probabilistic distributions for run-up extremes are not well defined in the literature, several methodological approaches can be taken to perform an analysis of extreme events. The joint probability method is widely used to account for the combined effects of different parameters influencing the run-up, such as wave height, wave period, and water levels. This approach evaluates the likelihood of simultaneous occurrences of these variables, providing a more thorough assessment of extreme events compared to analyzing each variable independently. A refinement of this method, the Direct Joint Probability Method (DJPM), directly evaluates the joint cumulative density function using the relative frequencies of combinations of contributing factors, such as tides, storm surges, and wave run-up. This approach allows for the inclusion of dependencies among these variables, overcoming the limitations of the traditional Joint Probability Method (JPM), which assumes independence between the factors (Liu et al., 2010).

The structural variable method uses measured wave parameters and water levels, applying a structural function to determine the quantity of interest (e.g., run-up). This method can predict quantities such as beach erosion, flooding extent, and seawall overtopping flow rate (Callaghan et al., 2008). By defining a deterministic relationship between input variables (wave and water level conditions) and the output variable (e.g., run-up), the structural function is integrated into probabilistic frameworks for extreme value analysis. Coupling this method with extreme value theory allows for the estimation of return levels and exceedance probabilities for the run-up parameter, enhancing coastal design and risk mitigation strategies. Additionally, this method is adaptable to site-specific conditions, as the structural function can be calibrated based on local morphological and hydrodynamic characteristics.

3.1.d Enhanced methodologies of landslide hazard assessment over network legs

3.1.d.1 Introduction

Landslides are complex natural phenomena that pose severe geohazards in many countries, occurring in diverse geological, geomorphological, and climatological environments. Thus, understanding the spatial and temporal distribution of landslides is crucial to assess related hazards and to support a comprehensive risk assessment (Grelle et al., 2014; Fusco et al., 2021; Fusco et al., 2023). The growing of urban settlements has led population settlement in areas at risk, where prediction and prevention actions are nowadays a challenge for geoscientists. In this context, landslide inventories can be used for various purposes, such as: preliminary step for the assessment of landslide susceptibility, hazard and risk. They are valuable for investigating landslide distribution, types and patterns in relation to morphological and geological factors as well as for studying landscape evolution. However, the practical utility of these inventories is often constrained by limited accessibility, spatial inhomogeneity or use of different mapping methods and classification criteria. This condition stands as a significant limitation for studies aimed at landslide susceptibility and risk assessment.

Landslide susceptibility assessment is the most common approach to assess how prone to landsliding is a landscape. Several methods and approaches, both qualitative and quantitative, have been proposed and tested for distributed landslide susceptibility assessment (Reichenbach et al., 2018). Assuming that "the past is the key to the future" (Carrara et al., 1995), the model learns how to distinguish the presence from the absence of a landslide based on a set of predisposing factors (i.e. slope degree, curvature, aspect, geology). For example, Titti et al. (2021) investigated how landslide presence variation affects the model performance by systematically reducing the number of the landslides in the dataset. The model performance has significantly improved in the last decade, particularly with the emergence of artificial intelligence-based models (Dahal et al., 2023), especially when the scale of the analysis is relatively small. However, landslide inventories still face limitations in terms of updating and accuracy (Titti et al. 2024).

3.1.d.2 Availability of national and regional landslide susceptibility and hazard maps

In Italy, many studies have already been conducted to map landslide susceptibility both at the basin scale and, less frequently, at the national scale. Among these, one of the most recent is the study presented by Loche et al. (2022). The aim of the study is to determine landslide susceptibility at the national scale for each type of landslide present in the territory, using a statistical methodology (Generalized Additive Model - INLA) based on the IFFI inventory.

In their work, Loche et al. (2022) use a division of the Italian territory into slope units created by CNR-IRPI of Perugia and described in the study by Alvioli et al. (2020). An added value compared to some previous studies conducted at the national scale is the preliminary work preceding the susceptibility analysis, which aims to assess the completeness of the landslide inventory. By comparing each regional inventory for individual types of landslides based on geomorphological units calculated by Alvioli et al. (2020), they highlighted a lack of homogeneity in the spatial distribution of events. This allowed them to identify regions with more detailed inventories compared to others, making them more suitable for training the statistical model.

3.1.d.3 Preliminary interaction assessment between landslide hazards and linear infrastructure at national scale

By comparing the results presented by Loche et al. (2022) with the network of Italian highways and railways, it is possible to identify sections of infrastructure located in areas susceptible to landslide events (Figure 5).

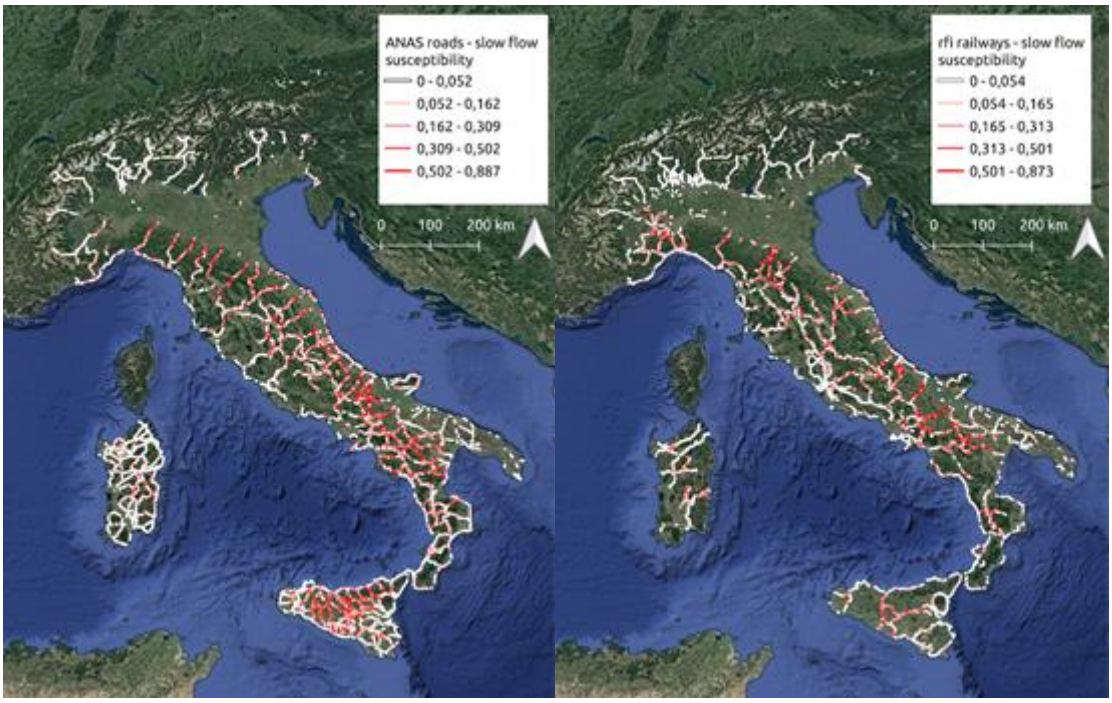

Figure 5: On the left, the distribution of susceptibility to 'slow flow' landslides relative to the road network managed by ANAS. On the right, the distribution of susceptibility to 'slow flow' landslides relative to the railway network.

3.1.d.4 Landslide hazard assessment in Calabria area

3.1.d.4.1 Study area

One of the Proof Of Concept (POC) selected by the Spoke TS2 is focused to investigate potential interaction between natural hazards and linear infrastructures. Based on a multi-hazard risk assessment, risk scenarios are evaluated considering slope instability, coastal erosion, river sediment transportation and wildfires.

The study area is located along the west Tyrrhenian coast of the Calabria Region from the town of Cittadella del Capo (Cosenza province) to Lamezia Terme (Catanzaro province). The area was considered representative because of the presence of an important railway (Napoli - Reggio Calabria line) and a primary road (SS18 Tirrena Inferiore) which developed along the coast. Such infrastructures are differently affected by all the natural hazards previously mentioned in terms of frequency and magnitude.

To understand in detail the problems of the study area and to compare the data present in literature with those in the field, a two day-long survey in the area in July 2024 has been conducted. This preliminary phase allowed to increase the knowledge about the geo-environmental conditions controlling the investigated hazards. Moreover, the risk prevention and mitigation measures taken by the infrastructure manager were investigated.

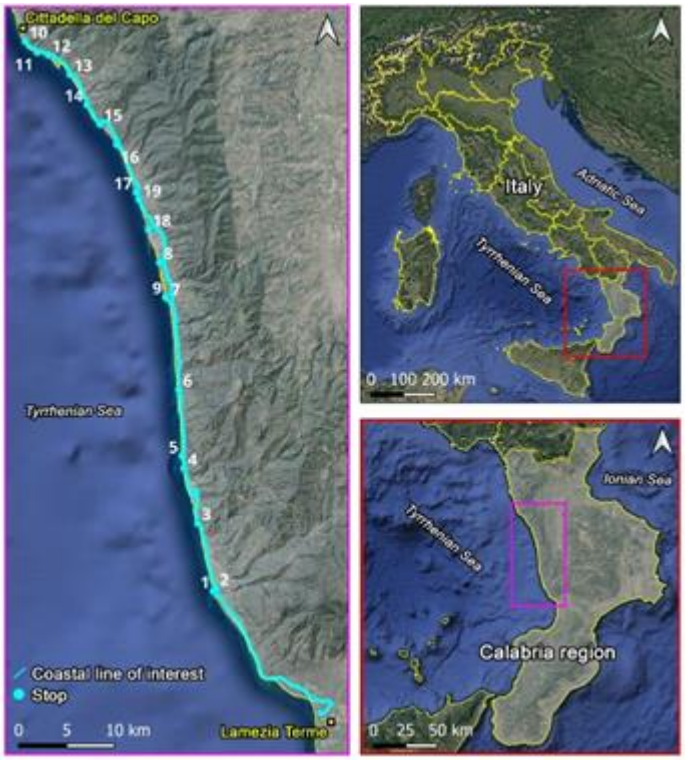

Figure 6: The area selected as Proof Of Concept in Calabria. About 100 km of coast is affected by slope instabilities, hydraulic hazard, coastal erosion, wildfires, tsunamis, and wind hazards.

3.1.d.4.2 Analysis and homogenization processing of available landslide inventories

The landslide inventories available for the study area are the IFFI and ITALICA catalogues and from local authorities.

The IFFI (Italian Landslide Inventory) is a comprehensive database of landslides compiled and regularly updated through the collaboration of national, regional, and provincial institutions (Trigila et al., 2010). It includes over 600,000 recorded landslides, with a total density of approximately 2 landslides per square kilometer, and occurrence dates spanning from 1116 to 2020. The data in the inventory were collected using various methods, including photo-interpretation, analysis of pre-existing records, and field surveys (Loche et al., 2022) (Figure 7).

Another national inventory of landslide is the ITALICA catalogue (ITAlian rainfall-induced LandslIdes CAtalogue) which includes 6312 records of rainfall-induced landslides between January 1996 and December 2021 with various spatial accuracy but more than one-third of the catalogue has a geographic accuracy less than 1 km^2 (Peruccacci et al., 2023) (Figure 7).

An additional inventory composed of 54 points of past landslides which affected the municipalities of the POC area have been provided by local authorities where no information about landslide type, trigger event or initiation date are available.

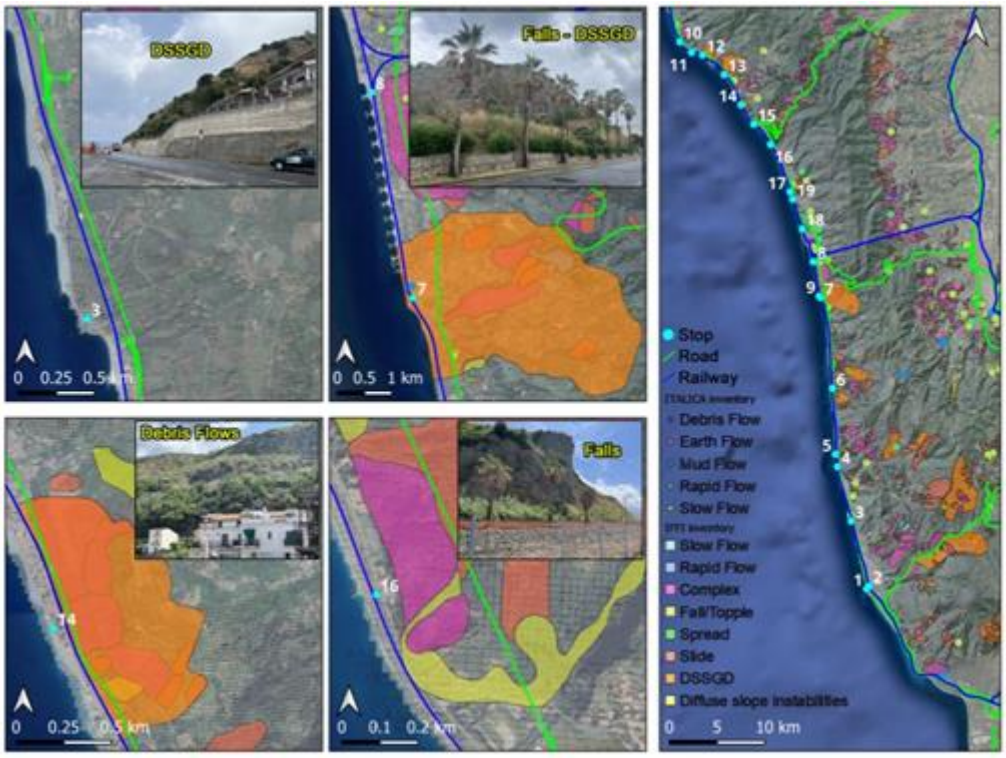

Figure 7: Landslide data from IFFI and ITALICA catalogues.

The inventories selected have been homogenized to face the classification proposed by the VS2 working group as reported in Figure 8.

Figure 8: Landslide classification based on RETURN Spoke VS2 proposal.Source: Spoke VS2 presentation.

3.1.d.4.3 Data collection for predisposing, preparatory and triggering factors

The predisposing, preparatory and triggering factors which drive each type of landslide have been established by the VS2 working group (see DV of VS2).

3.1.d.5.4 Application of the VS2 landslide tool chains

The application of the tool chains proposed by the VS2 working group is the core of the analysis. The tool chains developed differ according to the scale of application from local to regional. In the POC Calabria 4 different landslides have been selected to assess the interaction with the infrastructures at local/basin scale, while a single quantitative analysis at regional scale (entire POC area) will be performed to map the landslide susceptibility.

4. References

Abegaz, R., Xu, J., Wang, F., & Huang, J. (2024). Impact of flooding events on buried infrastructures: A review. Frontiers in Built Environment, 10, 1357741. https://doi.org/10.3389/fbuil.2024.1357741

Addor, N., Newman, A. J., Mizukami, N., & Clark, M. P. (2017). The CAMELS dataset: Catchment attributes and meteorology for large-sample studies. Hydrology and Earth System Sciences, 21, 5293–5313. https://doi.org/10.5194/hess-21-5293-2017

Alasia, A., Bollman, R. D., Parkins, J. R., & Reimer, B. (2017). Measuring remoteness and accessibility: a set of indices for Canadian communities. Canadian Journal of Regional Science, 40(1), 1–15.

Albertini, C., Gioia, A., Iacobellis, V., & Manfreda, S. (2022). Detection of surface water and floods with multispectral satellites. Remote Sensing, 14(23), 6005. https://doi.org/10.3390/rs14236005

Alexander, D. C., Zikic, D., Zhang, J., Zhang, H., & Criminisi, A. (2014). Image Quality Transfer via Random Forest Regression: Applications in Diffusion MRI. In P. Golland, N. Hata, C. Barillot, J. Hornegger, & R. Howe (Eds.), Medical Image Computing and Computer-Assisted Intervention – MICCAI 2014 (Vol. 8675, pp. 225–232). Springer International Publishing. https://doi.org/10.1007/978-3-319-10443-0_29

Alvioli, M., Guzzetti, F., & Marchesini, I. (2020). Parameter-free delineation of slope units and terrain subdivision of Italy. Geomorphology, 358, 107124. https://doi.org/10.1016/j.geomorph.2020.107124

Apel, H., Merz, B., & Thieken, A. H. (2009). Influence of dike breaches on flood frequency estimation. Computers & Geosciences, 35(5), 907–923. https://doi.org/10.1016/j.cageo.2007.11.003

Avand, M., Kuriqi, A., Khazaei, M., & Ghorbanzadeh, O. (2022). DEM resolution effects on machine learning performance for flood probability mapping. Journal of Hydro-Environment Research, 40, 1–16. https://doi.org/10.1016/j.jher.2021.10.002

Bíl, M., Vodák, R., Kubecek, J., Bílová, M., & Sedoník, J. (2015). Evaluating road network damage caused by natural disasters in the Czech Republic between 1997 and 2010. Transportation Research Part A: Policy and Practice, 80, 90–103. https://doi.org/10.1016/j.tra.2015.07.006

Bozzo, E., & Franceschet, M. (2013). Resistance distance, closeness, and betweenness. Social Networks, 35(3), 460–469. https://doi.org/10.1016/j.socnet.2013.05.003

Braca, G., Bussettini, M., Lastoria, B., Mariani, S., & Piva, F. (2021). Elaborazioni modello BIGBANG versione 4.0. Istituto Superiore per la Protezione e la Ricerca Ambientale – ISPRA, http://groupware.sinanet.isprambiente.it/bigbang-data/library/bigbang40

Brath, A., & Montanari, A. (2000). Vulnerabilità idraulica dei ponti. L'Acqua, 3.

Breiman, L. (1996). Bagging predictors. Machine Learning, 24(2), 123–140. https://doi.org/10.1007/BF00058655

Breiman, L. (2001). Random Forests. Machine Learning, 45(1), 5–32. https://doi.org/10.1023/A:1010933404324

Bui, D. T., Tsangaratos, P., Ngo, P.-T. T., Pham, T. D., & Pham, B. T. (2019). Flash flood susceptibility modeling using an optimized fuzzy rule based feature selection technique and tree based ensemble methods. Science of The Total Environment, 668, 1038–1054. https://doi.org/10.1016/j.scitotenv.2019.02.422

Bui, Q.-T., Nguyen, Q.-H., Nguyen, X. L., Pham, V. D., Nguyen, H. D., & Pham, V.-M. (2020). Verification of novel integrations of swarm intelligence algorithms into deep learning neural network for flood susceptibility mapping. Journal of Hydrology, 581, 124379. https://doi.org/10.1016/j.jhydrol.2019.124379

Buonora, L., Moccia, B., Ridolfi, E., Russo, F., & Napolitano, F. (2024). Safety assessment of bridges: Analysis and criticalities of the guidelines for hydraulic risk management. Procedia Structural Integrity, 62, 647–652. https://doi.org/10.1016/j.prostr.2024.09.090

Callaghan, D. P., Nielsen, P., Short, A., & Ranasinghe, R. W. M. R. J. B. (2008). Statistical simulation of wave climate and extreme beach erosion. Coastal Engineering, 55(5), 375–390.

Carrara, A., Cardinali, M., Guzzetti, F., & Reichenbach, P. (1995). GIS technology in mapping landslide hazard. Geographical Information Systems in Assessing Natural Hazards. Springer: Dordrecht, The Netherland, 135-175.

Carriero, D. (2024). Analisi della distribuzione delle caratteristiche idrologiche dei suoli per applicazioni di modelli di simulazione afflussi-deflussi. PhD thesis, Università degli studi della Basilicata.

Carter, R. (1961). Magnitude and frequency of floods in suburban areas. In: Short papers in the geologic and hydrologic sciences, U.S. geol. Survey. Prof. paper 424-B, B9-B11

Chang, H., Lafrenz, M., Jung, I.-W., Figliozzi, M., Platman, D., & Pederson, C. (2010). Potential impacts of climate change on flood-induced travel disruptions: A case study of Portland, Oregon, USA. Annals of the Association of American Geographers, 100(4), 938–952. https://doi.org/10.1080/00045608.2010.497110

Chang, K.-T., Merghadi, A., Yunus, A. P., Pham, B. T., & Dou, J. (2019). Evaluating scale effects of topographic variables in landslide susceptibility models using GIS-based machine learning techniques. Scientific Reports, 9(1), 12296. https://doi.org/10.1038/s41598-019-48773-2

Chen, X.-Z., Lu, Q.-C., Peng, Z.-R., & Ash, J. E. (2015). Analysis of transportation network vulnerability under flooding disasters. Transportation Research Record: Journal of the Transportation Research Board, 2532(1), 37–44. https://doi.org/10.3141/2532-05

Chen, L. L., Wang, Z. F., & Wang, Y.Q (2022). Failure analysis and treatments of tunnel entrance collapse due to sustained rainfall: a case study. Water, 14, 16, 2486. https://doi.org/10.3390/W14162486

Cho, H. (2020). A recursive algorithm for calculating the longest flow path and its iterative implementation. Environmental Modelling & Software, 131, 104774. https://doi.org/10.1016/j.envsoft.2020.104774

Chow, V. T. (1959). Open-channel hydraulics. McGraw-Hill.

Chow, V. T. (1962). Hydrologic determination of waterway areas for the design of drainage structures in small drainage basins. University of Illinois Engineering Experiment Station Bulletin No. 462, Urbana, IL.

CIMA Research Foundation & Internal Displacement Monitoring Centre (2024). Floods and drought displacement risk in Ethiopia, Somalia, and Sudan (HABITABLE research paper). Geneva: IDMC.

Claps, P., Ganora, D., Apostolo, A., Brignolo, I., & Monforte, I. (2020a). Catalogo delle Piene dei Corsi d'acqua Italiani Vol. 1. Ed. CINID., 499 pp., ISBN 978-88-945568-0-3.

Claps, P., Ganora, D., Apostolo, A., Brignolo, I., & Monforte, I. (2020b). Catalogo delle Piene dei Corsi d'acqua Italiani Vol. 2. Ed. CINID, 537 pp., ISBN 978-88-945568-2-7.

Claps, P., Ganora, D., Apostolo, A., Brignolo, I., & Monforte, I. (2020c). Catalogo delle Piene dei Corsi d'acqua Italiani Vol. 3. Ed. CINID, 401 pp., ISBN 978-88-945568-4-1.

Claps, P., Evangelista, G., Ganora, D., Mazzoglio, P., & Monforte, I. (2024). FOCA: A new quality-controlled database of floods and catchment descriptors in Italy. Earth System Science Data, 16, 1503–1522. https://doi.org/10.5194/essd-16-1503-2024

Codato, C., Castellino, M., Pasquali, D., Di Risio, M., Scipione, F., Ruffini, G., & De Girolamo, P. (2024). Climate change impact on extreme wave conditions off Italian coasts. XXXIX Convegno Nazionale di Idraulica e Costruzioni Idrauliche (IDRA2024), Parma, 15-18 September 2024, Università degli Studi di Parma - Dipartimento di Ingegneria e Architettura, pp. 1473-1476. https://doi.org/10.5281/zenodo.13584918

Cohen, J. (1988). Statistical power analysis for the behavioral sciences (2nd ed). L. Erlbaum Associates.

Coles, S., Bawa, J., Trenner, L., & Dorazio, P. (2001). An introduction to statistical modeling of extreme values (Vol. 208, p. 208). London: Springer.

Dahal, A. & Lombardo, L. (2023). Explainable artificial intelligence in geoscience: a glimpse into the future of landslide susceptibility modeling. Computers & Geosciences, 176, 105364.

Dai, B., Chen, R.-C., Zhu, S.-Z., & Zhang, W.-W. (2018). Using Random Forest Algorithm for Breast Cancer Diagnosis. 2018 International Symposium on Computer, Consumer and Control (IS3C), 449–452. https://doi.org/10.1109/IS3C.2018.00119

Dawson, R., Hall, J., Sayers, P., Bates, P., & Rosu, C. (2005). Sampling-based flood risk analysis for fluvial dike systems. Stochastic Environmental Research and Risk Assessment, 19(5), 388–402. https://doi.org/10.1007/s00477-005-0193-0

Dijkstra, E. W. (1959). A note on two problems in connexion with graphs. Numerische Mathematik, 1, 269–271.

Dong, S., Esmalian, A., Farahmand, H., & Mostafavi, A. (2020). An integrated physical-social analysis of disrupted access to critical facilities and community service-loss tolerance in urban flooding. Computers, Environment and Urban Systems, 80, 101443. https://doi.org/10.1016/j.compenvurbsys.2019.101443

Dong, W., Huang, H., Zhong, M., & Long, Z. (2024). Experimental study on the inundation characteristics of flooding in a long straight subway tunnel. Tunnelling and Underground Space Technology, 144, 105566. https://doi.org/10.1016/J.TUST.2023.105566

Du, P., Samat, A., Waske, B., Liu, S., & Li, Z. (2015). Random Forest and Rotation Forest for fully polarized SAR image classification using polarimetric and spatial features. ISPRS Journal of Photogrammetry and Remote Sensing, 105, 38–53. https://doi.org/10.1016/j.isprsjprs.2015.03.002

El-Haddad, B. A., Youssef, A. M., Pourghasemi, H. R., Pradhan, B., El-Shater, A.-H., & El-Khashab, M. H. (2021). Flood susceptibility prediction using four machine learning techniques and comparison of their performance at Wadi Qena Basin, Egypt. Natural Hazards, 105(1), 83–114. https://doi.org/10.1007/s11069-020-04296-y

Eppstein, D. (1998). Finding the k shortest paths. SIAM Journal on Computing, 28(2), 652–673.

Fannin, R. J., & Wise, M. P. (2001). An empirical-statistical model for debris flow travel distance. Canadian Geotechnical Journal, 38(5), 982–994.

Farr, T. G., Rosen, P. A., Caro, E., Crippen, R., Duren, R., Hensley, S., Kobrick, M., Paller, M., Rodriguez, E., Roth, L., Seal, D., Shaffer, S., Shimada, J., Umland, J., Werner, M., Oskin, M., Burbank, D., & Alsdorf, D. (2007). The Shuttle Radar Topography Mission. Reviews of Geophysics, 45, RG2004. https://doi.org/10.1029/2005RG000183

Fell, R., Wan, C. F., Cyganiewicz, J., & Foster, M. (2003). Time for development of internal erosion and piping in embankment dams. Journal of Geotechnical and Geoenvironmental Engineering, 129(4), 307–314. https://doi.org/10.1061/(ASCE)1090-0241(2003)129:4(307)

Firmi, P., Iacobini, F., Rinaldi, A., Vecchi, A., Agostino, I., & Mauro, A. (2021). Methods for managing hydrogeological and seismic hazards on the Italian railway infrastructure. Structure and Infrastructure Engineering, 17(12), 1651–1666. https://doi.org/10.1080/15732479.2020.1822883

Freeman, L. C. (1977). A set of measures of centrality based on betweenness. Sociometry, 40(1), 35-41.

Fusco, F., Mirus, B. B., Baum, R. L., Calcaterra, D. & De Vita, P. (2021). Incorporating the effects of complex soil layering and thickness local variability into distributed landslide susceptibility assessments. Water, 13, 713.

Fusco, F., Abbate, A., Calcaterra, D., De Vita, P., Guerriero, L., Longoni, L. & Papini, M. (2023). Susceptibility mapping of shallow landslides inducing debris flows: a comparison of physics-based approaches. Italian Journal of Engineering Geology and Environment, 1, 63-71.

Grelle, G., Soriano, M., Revellino, P., Guerriero, L., Anderson, M. G., Diambra, A., Fiorillo, F., Esposito, L., Diodato, N., & Guadagno, F. M. (2014). Space-time prediction of rainfall-induced shallow landslides through a combined probabilistic/deterministic approach, optimized for initial water table conditions. Bulletin of Engineering Geology and the Environment, 73, 877-890.

Gschnitzer, T., Gems, B., Mazzorana, B., & Aufleger, M. (2017). Towards a robust assessment of bridge clogging processes in flood risk management. Geomorphology, 279, 128-140.

Hao, Z., Jin, J., Xia, R., Tian, S., Yang, W., Liu, Q., Zhu, M., Ma, T., Jing, C., & Zhang, Y. (2021). CCAM: China Catchment Attributes and Meteorology dataset. Earth System Science Data, 13, 5591–5616. https://doi.org/10.5194/essd-13-5591-2021

Hengl, T., Mendes de Jesus, J., Heuvelink, G. B. M., Ruiperez Gonzalez, M., Kilibarda, M., Blagotic, A., Shangguan, W., Wright, M. N., Geng, X., Bauer-Marschallinger, B.,Guevara, M. A., Vargas, R., MacMillan, R. A., Batjes, N. H., Leenaars, J. G. B., Ribeiro, E.,Wheeler, I., Mantel, S., & Kempen, B. (2017). SoilGrids250m: global gridded soil information based on machine learning. PLOS ONE, 12, e0169748. https://doi.org/10.1371/journal.pone.0169748

Hersbach, H., Bell, B., Berrisford, P., Hirahara, S., Horányi, A., Muñoz-Sabater, J., & Thépaut, J. N. (2020). The ERA5 global reanalysis. Quarterly Journal of the Royal Meteorological Society, 146(730), 1999-2049.

Hiemstra, P., & Skoien, J. O. (2023). Package "automap". https://cran.r-project.org/web/packages/automap/automap.pdf

Jacobs, J. M., Cattaneo, L. R., Sweet, W., & Mansfield, T. (2018). Recent and future outlooks for nuisance flooding impacts on roadways on the U.S. East Coast. Transportation Research Record, 2672(2), 1–10. https://doi.org/10.1177/0361198118756366

Japanese Geotechnical Society (2006). Ground damage resulting from torrential rains in Fukui, July 2004, Emergency Survey Team, Soils and Foundations, 46, 869–884.

Jasiewicz, J. (2021). r.stream.stats. https://grass.osgeo.org/grass82/manuals/addons/r.stream.stats.html

Jowett, I. G. (1998). Hydraulic geometry of New Zealand rivers and its use as a preliminary method of habitat assessment. Regulated Rivers: Research & Management, 14, 451–466. https://doi.org/10.1002/(SICI)1099-1646(1998090)14:5%3C451::AID-RRR512%3E3.0.CO;2-1

Khosravi, K., Nohani, E., Maroufinia, E., & Pourghasemi, H. R. (2016). A GIS-based flood susceptibility assessment and its mapping in Iran: A comparison between frequency ratio and weights-of-evidence bivariate statistical models with multi-criteria decision-making technique. Natural Hazards, 83(2), 947–987. https://doi.org/10.1007/s11069-016-2357-2

Khosravi, K., Pham, B. T., Chapi, K., Shirzadi, A., Shahabi, H., Revhaug, I., Prakash, I., & Tien Bui, D. (2018). A comparative assessment of decision trees algorithms for flash flood susceptibility modeling at Haraz watershed, northern Iran. Science of The Total Environment, 627, 744–755. https://doi.org/10.1016/j.scitotenv.2018.01.266

Khosravi, K., Shahabi, H., Pham, B. T., Adamowski, J., Shirzadi, A., Pradhan, B., Dou, J., Ly, H.-B., Gróf, G., Ho, H. L., Hong, H., Chapi, K., & Prakash, I. (2019). A comparative assessment of flood susceptibility modeling using Multi-Criteria Decision-Making Analysis and Machine Learning Methods. Journal of Hydrology, 573, 311–323. https://doi.org/10.1016/j.jhydrol.2019.03.073

Kia, M. B., Pirasteh, S., Pradhan, B., Mahmud, A. R., Sulaiman, W. N. A., & Moradi, A. (2012). An artificial neural network model for flood simulation using GIS: Johor River Basin, Malaysia. Environmental Earth Sciences, 67(1), 251–264. https://doi.org/10.1007/s12665-011-1504-z

Kirpich, Z. (1940). Time of concentration of small agricultural watersheds. Civ. Eng. 10(6), 362.

Klingler, C., Schulz, K., & Herrnegger, M. (2021). LamaH-CE: LArge-SaMple DAta for Hydrology and Environmental Sciences for Central Europe. Earth System Science Data, 13, 4529–4565. https://doi.org/10.5194/essd-13-4529-2021

Koks, E. E., Rozenberg, J., Zorn, C., Tariverdi, M., Vousdoukas, M., Fraser, S. A., & Hallegatte, S. (2019). A global multi-hazard risk analysis of road and railway infrastructure assets. Nature Communications, 10, 2677. https://doi.org/10.1038/s41467-019-10442-3

Koks, E., Rozenberg, J., Tariverdi, M., Dickens, B., Fox, C., van Ginkel, K. & Hallegatte, S. (2023) A global assessment of national road network vulnerability. Environmental Research: Infrastructure and Sustainability, 3, 025008. https://doi.org/10.1088/2634-4505/acd1aa

Kratzert, F., Nearing, G., Addor, N., Erickson, T., Gauch, M., Gilon, O., Gudmundsson, L., Hassidim, A., Klotz, D., Nevo, S., Shalev, G., & Matias, Y. (2023). Caravan - A global community dataset for large-sample hydrology. Scientific Data, 10, 61. https://doi.org/10.1038/s41597-023-01975-w

Khosravi, K., Shahabi, H., Pham, B. T., Adamowski, J., Shirzadi, A., Pradhan, B., Dou, J., Ly, H.-B., Gróf, G., Ho, H. L., Hong, H., Chapi, K., & Prakash, I. (2019). A comparative assessment of flood susceptibility modeling using Multi-Criteria Decision-Making Analysis and Machine Learning Methods. Journal of Hydrology, 573, 311–323. https://doi.org/10.1016/j.jhydrol.2019.03.073

Kulkarni, A. D., & Lowe, B. (2016). Random Forest Algorithm for Land Cover Classification. International Journal on Recent and Innovation Trends in Computing and Communication, 4(3).

Lai, H., Song, W., Liu, Y., & Chen, R. (2017). Influence of flooded loessial overburden on the tunnel lining: Case study. Journal of Performance of Constructed Facilities, 31(6), 04017108. https://doi.org/10.1061/(ASCE)CF.1943-5509.0001100

Lane, E. W. (1934). Security from under-seepage masonry dams on earth foundations. Transactions of the American Society of Civil Engineers, 60(4), 929–966.

Leopold, L. B. (1953). Downstream change of velocity in rivers. American Journal of Science, 251, 606-624. https://doi.org/10.2475/ajs.251.8.606

Leopold, L. B., & Maddock, T. (1953). The Hydraulic Geometry of Stream Channels and Some Physiographic Implications. Geological Survey Professional Paper 252.

Li, Z., Gao, S., Chen, M., Gourley, J. J., Liu, C., Prein, A. F., & Hong, Y. (2022). The Conterminous United States are projected to become more prone to flash floods in a high-end emissions scenario. https://doi.org/10.1038/s43247-022-00409-6

Lin, H., Li, G., Yu, Y., & Lu., H. (1936). Influence of Matric Suction on Shear Strength Behavior of Unsaturated Soils. Rock Soil Mech, no. 09: 2007.

Lindsay, J. B. & Creed, I. F. (2005). Removal of artifact depressions from digital elevation models: towards a minimum impact approach. Hydrological Process., 19, 3113–3126, https://doi.org/10.1002/hyp.5835

Liu, J. C., Lence, B. J., & Isaacson, M. (2010). Direct joint probability method for estimating extreme sea levels. Journal of Waterway, Port, Coastal, and Ocean Engineering, 136(1), 66–76. https://doi.org/10.1061/(ASCE)0733-950X(2010)136:1(66)

Loche, M., Alvioli, M., Marchesini, I., Bakka, H., & Lombardo, L. (2022). Landslide susceptibility maps of Italy: lesson learnt from dealing with multiple landslide types and the uneven spatial distribution of the national inventory. Earth-Science Reviews, 232, 104125.

Ma, Y., Yang, J., Li, L., & Li, Y. (2022). Analysis on ultimate water pressure and treatment measures of tunnels operating in water rich areas based on water hazard investigation. Alexandria Engineering Journal 61, 8, 6581–89. https://doi.org/10.1016/J.AEJ.2021.11.040

Mahmood, K., Kim, J. M., Khan, H., Safdar, M., & Khan, U. (2018). The probabilistic stability analysis of saturated-unsaturated MH and CL soil slope with rainfall infiltration. KSCE Journal of Civil Engineering 22, 5, 1742–49. https://doi.org/10.1007/s12205-017-1052-5

Manfreda, S., Samela, C. (2019). A digital elevation model based method for a rapid estimation of flood inundation depth. J. Flood Risk Manag., 12, e12541. https://doi.org/10.1111/jfr3.12541

Manfreda, S., Samela, C., Gioia, A., Consoli, G.G., Iacobellis, V., Giuzio, L., Cantisani, A., & Sole, A. (2015). Flood-prone areas assessment using linear binary classifiers based on flood maps obtained from 1D and 2D hydraulic models. Nat. Hazards 79, 735–754. https://doi.org/10.1007/s11069-015-1869-5

Mas, E., Koshimura, S., Suppasri, A., Matsuoka, M., Matsuyama, M., Yoshii, T., Jimenez, C., Yamazaki, F., & Imamura, F. (2012). Developing Tsunami fragility curves using remote sensing and survey data of the 2010 Chilean Tsunami in Dichato. Natural and Hazards Earth System Sciences, 12, 2689–2697, https://doi.org/10.5194/nhess-12-2689-2012

Mazzoglio, P., Butera, I., & Claps, P. (2020). I^2-RED: a massive update and quality control of the Italian annual extreme rainfall dataset. Water, 12, 3308, https://doi.org/10.3390/w12123308

McCuen, R.H., Wong, S., & Rawls, W. (1984). Estimating urban time of concentration. J. Hydraulic Eng. Am. Society Civil Engineers, 110, 887-904.

Meinshausen, M., Smith, S. J., Calvin, K., Daniel, J. S., Kainuma, M. L., Lamarque, J. F., Matsumoto, K., Montzka, S. A., Raper, S. C. B., Riahi, K., Thomson, A., Velders, G. J. M., & van Vuuren, D. P. (2011). The RCP greenhouse gas concentrations and their extensions from 1765 to 2300. Climatic Change, 109, 213-241.

Mohammady, M., Pourghasemi, H. R., & Amiri, M. (2019). Land subsidence susceptibility assessment using random forest machine learning algorithm. Environmental Earth Sciences, 78(16), 503. https://doi.org/10.1007/s12665-019-8518-3

Morucci, S., Picone, M., Nardone, G., & Arena, G. (2016). Tides and waves in the Central Mediterranean Sea, Journal of Operational Oceanography, 9:sup1, s10-s17. https://doi.org/10.1080/1755876X.2015.1120960

Motta, M., de Castro Neto, M., & Sarmento, P. (2021). A mixed approach for urban flood prediction using Machine Learning and GIS. International Journal of Disaster Risk Reduction, 56, 102154. https://doi.org/10.1016/j.ijdrr.2021.102154

Nachappa, T., Tavakkoli Piralilou, S., Gholamnia, K., Ghorbanzadeh, O., Rahmati, O., & Blaschke, T. (2020). Flood susceptibility mapping with machine learning, multi-criteria decision analysis and ensemble using Dempster Shafer Theory. Journal of Hydrology, 590, 125275. https://doi.org/10.1016/j.jhydrol.2020.125275

Nardi, F., Annis, A., Di Baldassarre, G., Vivoni, E. R., & Grimaldi, S. (2019). GFPLAIN250m, a global high-resolution dataset of Earth's floodplains. Scientific Data, 6(1), 180309. https://doi.org/10.1038/sdata.2018.309

Néelz, S., & Pender, G. (2010). Benchmarking of 2D hydraulic modelling packages. https://www.semanticscholar.org/paper/Benchmarking-of-2D-hydraulic-modelling-packages-N%C3%A9elz-Pender/67ed561d40c4ce20ed5984d1e28f56d1e62bb31a

Néelz, S., & Pender, G. (2013). Delivering benefits thorough evidences: benchmarking the latest generation of 2D hydraulic modelling packages. Report—SC120002.4

Newman, M. E. J. (2010). Networks: an introduction. Oxford University Press.

Oshiro, T. M., Perez, P. S., & Baranauskas, J. A. (2012). How Many Trees in a Random Forest? In P. Perner (Ed.), Machine Learning and Data Mining in Pattern Recognition (pp. 154–168). Springer. https://doi.org/10.1007/978-3-642-31537-4_13

Pant, R., Thacker, S., Hall, J., Barr, S., & Alderson, D. (2016). Critical infrastructure impact assessment due to flood exposure. Journal of Flood Risk Management, 11(1), 22–33. https://doi.org/10.1111/jfr3.12288

Papilloud, T., Sahin, O., & Stewart, R. A. (2021). A comprehensive review of accessibility measures in transport resilience studies. Transport Reviews, 41(5), 618–639.

Pasquali, D., Bruschi, A., Lisi, I., & Risio, M. D. (2023). Wave Forcing Assessment at Regional Scale in a Climate Change Scenario: The Sardinia Case Study. Journal of Marine Science and Engineering, 11(9), 1786.

Pastorello, R., Michelini, T., & d'Agostino, V. (2017). Erratum to: On the criteria to create a susceptibility map to debris flow at a regional scale using Flow-R. Journal of Mountain Science, 14(5), 1008. https://doi.org/10.1007/s11629-017-4389-9

Peng, S. C., Zhou, Y. M., Cao, L. H., Yu, S., Niu, J. W., & Jia, W. J. (2018). Influence analysis in social networks: A survey. Journal of Network and Computer Applications, 106, 17–32.

Peruccacci, S., Gariano, S. L., Melillo, M., Solimano, M., Guzzetti, F., & Brunetti, M. T. (2023). ITALICA, an extensive and accurate spatio-temporal catalogue of rainfall-induced landslides in Italy. Earth System Science Data Discussions, 2023, 1-24.

Pilgrim, D. H. (1977). Isochrones of travel time and distribution of flood storage from a tracer study on a small watershed. Water Resources Research, 13(3). https://doi.org/10.1029/WR013i003p00587

Polemio, M., & Lollino, P. (2011). Failure of infrastructure embankments induced by flooding and seepage: A neglected source of hazard. Natural Hazards and Earth System Sciences, 11(12), 3383–3396. https://doi.org/10.5194/nhess-11-3383-2011

Pörtner, H. O., Roberts, D. C., Masson-Delmotte, V., Zhai, P., Tignor, M., Poloczanska, E., & Weyer, N. M. (2019). The ocean and cryosphere in a changing climate. In IPCC Special Report on the Ocean and Cryosphere in a Changing Climate; IPCC: Geneva, Switzerland, Vol. 1155.

Priest, S., Wilson, T., Tapsell, S., Penning-Rowsell, E., Viavattene, C., & Fernandez-Bilbao, A. (2007). Building a model to estimate risk to life for European flood events – Final report. FLOODsite.

Prudhomme, C., & Genevier, M. (2011). Can atmospheric circulation be linked to flooding in Europe? Hydrological Processes, 25(7), 1180–1190. https://doi.org/10.1002/hyp.7879

Tsubaki, R., Bricker, J. D., Ichii, K., & Kawahara, Y. (2016). Development of fragility curves for railway embankment and ballast scour due to overtopping flood flow. Natural Hazards and Earth System Sciences, 16, 2455–2472.

Radovanović, S., Milivojević, M., Stojanović, B., Obradović, S., Divac, D., & Milivojević, N. (2022). Modeling of water losses in hydraulic tunnels under pressure based on stepwise regression method. Applied Sciences, 12(18), 9019. https://doi.org/10.3390/app12189019

RED Engineering (2022). Task 5b - Flood vulnerability - Regionally consistent risk assessment for earthquakes and floods and selective landslide scenario analysis for strengthening financial resilience and accelerating risk reduction in Central Asia (SFRARR Central Asia disaster risk assessment). Technical Assignment Number 1266456.

Reichenbach, P., Rossi, M., Malamud, B. D., Mihir, M., & Guzzetti, F. (2018). A review of statistically–based landslide susceptibility models. Earth Sci. Rev, 180, 60-91.

Rice, M. E., & Harris, G. T. (2005). Comparing effect sizes in follow-up studies: ROC Area, Cohen's d, and r. Law and Human Behavior, 29(5), 615–620. https://doi.org/10.1007/s10979-005-6832-7

Rodriguez-Galiano, V. F., Ghimire, B., Rogan, J., Chica-Olmo, M., & Rigol-Sanchez, J. P. (2012). An assessment of the effectiveness of a random forest classifier for land-cover classification. ISPRS Journal of Photogrammetry and Remote Sensing, 67, 93–104. https://doi.org/10.1016/j.isprsjprs.2011.11.002

Rudari, R., Abbashar, A., Conijn, S., de Moel, H., Denis-Loupot, A., Ferraris, L., et al. (2019). UR Tanzania disaster risk profile. Nairobi: UNDRR and CIMA Research Foundation.

Samela, C., Manfreda, S., De Paola, F., Giugni, M., Sole, A., & Fiorentino, M. (2016). DEM-Based Approaches for the Delineation of Flood-Prone Areas in an Ungauged Basin in Africa. J. Hydrol. Eng. 21, 6015010. https://doi.org/10.1061/(ASCE)HE.1943-5584.0001272

Samela, C., Troy, T.J., & Manfreda, S. (2017). Geomorphic classifiers for flood-prone areas delineation for data-scarce environments. Adv. Water Resour. 102, 13–28.

Samela, C., Albano, R., Sole, A., & Manfreda, S. (2018). A GIS tool for cost-effective delineation of flood-prone areas. Comput. Environ. Urban Syst., 70, 43–52.

Samela, C., Carisi, F., Domeneghetti, A., Petruccelli, N., Castellarin, A., Iacobini, F., et al. (2023). A methodological framework for flood hazard assessment for land transport infrastructures. International Journal of Disaster Risk Reduction, 85, 103491. https://doi.org/10.1016/j.ijdrr.2022.103491

Saxton, K. E., Rawls, W. J., Romberger, J. S., & Papendick, R. I. (1986). Estimating generalized soil-water characteristics from texture. Soil Science Society of America Journal, 50, 1031–1036. https://doi.org/10.2136/sssaj1986.03615995005000040039x

Schonlau, M., & Zou, R. Y. (2020). The random forest algorithm for statistical learning. The Stata Journal: Promoting Communications on Statistics and Stata, 20(1), 3–29. https://doi.org/10.1177/1536867X20909688

Serre, D., & Heinzlef, C. (2018). Assessing and mapping urban resilience to floods with respect to cascading effects through critical infrastructure networks. International Journal of Disaster Risk Reduction, 30, 235–243. https://doi.org/10.1016/j.ijdrr.2018.02.018

Sharifi, S., & Hosseini, S. M. (2011). Methodology for identifying the best equations for estimating the time of concentration of watersheds in a particular region. Journal of Irrigation and Drainage Engineering, 137(11), 685–746. https://doi.org/10.1061/(ASCE)IR.1943-4774.0000373

Sheridan, J. M. (1994). Hydrograph time parameters for flatland watersheds. Transactions of the American Society of Agricultural Engineers 37(1), 103–113. https://doi.org/10.13031/2013.28059

Sherman, L. K. (1932). Streamflow from rainfall by the unit-graph method. Eng. News Record, 108, 501-505.

Shi, T., & Horvath, S. (2006). Unsupervised Learning With Random Forest Predictors. Journal of Computational and Graphical Statistics, 15(1), 118–138. https://doi.org/10.1198/106186006X94072

Shinozuka, M., Feng, M. Q., Lee, J., & Naganuma, T. (2000). Statistical analysis of fragility curves. Journal of Engineering Mechanics, 126, 1224–1231. https://doi.org/10.1061/(ASCE)0733-9399(2000)126:11(1224)

Shook, K. R., Whitfield, P. H., Spence, C., & Pomeroy, J. W. (2024). Estimating response times, flow velocities, and roughness coefficients of Canadian Prairie basins. Hydrology and Earth System Sciences, 28, 5173–5192. https://doi.org/10.5194/hess-28-5173-2024

Siregar, R. I., Nursyamsi, N., Indrawan, I., Sembiring, R. A., Karolina, R., Dewi, R. A. (2020). Integrated Systems of Major Drainage and Minor Drainage towards Low Impact Development. IOP Conference Series: Materials Science and Engineering, 801, 1, 012021. https://doi.org/10.1088/1757-899X/801/1/012021

Soil Conservation Service (1972). National engineering handbook, section 4: Hydrology. Department of Agriculture, Washington, DC.

Straub, L. G. (1934). Effect of channel contraction works upon regimen of movable bed streams. Transactions of the American Geophysical Union, Part 2, 454–463.

Suppasri, A., Mas, E., Koshimura, S., Imai, K., Harada, K., & Imamura, F. (2012). Developing tsunami fragility curves from the surveyed data of the 2011 Great East Japan tsunami in Sendai and Ishinomaki plains. Coastal Engineering Journal, 54, 1250008. https://doi.org/10.1142/S0578563412500088

Tang, F., & Ishwaran, H. (2017). Random forest missing data algorithms. Statistical Analysis and Data Mining: The ASA Data Science Journal, 10(6), 363–377. https://doi.org/10.1002/sam.11348

Tavares da Costa, R., Zanardo, S., Bagli, S., Hilberts, A. G. J., Manfreda, S., Samela, C., & Castellarin, A. (2020). Predictive Modeling of Envelope Flood Extents Using Geomorphic and Climatic-Hydrologic Catchment Characteristics. Water Resources Research, 56(9), e2019WR026453. https://doi.org/10.1029/2019WR026453

Taylor, M. A. P., & Susilawati (2012). Remoteness and accessibility in the vulnerability analysis of regional road networks. Transportation Research Part A: Policy and Practice, 46(5), 761–771. https://doi.org/10.1016/j.tra.2012.02.008

Tehrany, M. S., Pradhan, B., & Jebur, M. N. (2013). Spatial prediction of flood susceptible areas using rule based decision tree (DT) and a novel ensemble bivariate and multivariate statistical models in GIS. Journal of Hydrology, 504, 69–79. https://doi.org/10.1016/j.jhydrol.2013.09.034

Tehrany, M. S., Lee, M.-J., Pradhan, B., Jebur, M. N., & Lee, S. (2014a). Flood susceptibility mapping using integrated bivariate and multivariate statistical models. Environmental Earth Sciences, 72(10), 4001–4015. https://doi.org/10.1007/s12665-014-3289-3

Tehrany, M. S., Pradhan, B., & Jebur, M. N. (2014b). Flood susceptibility mapping using a novel ensemble weights-of-evidence and support vector machine models in GIS. Journal of Hydrology, 512, 332–343. https://doi.org/10.1016/j.jhydrol.2014.03.008

Tehrany, M. S., Pradhan, B., Mansor, S., & Ahmad, N. (2015). Flood susceptibility assessment using GIS-based support vector machine model with different kernel types. CATENA, 125, 91–101. https://doi.org/10.1016/j.catena.2014.10.017

Tehrany, M. S., Jones, S., & Shabani, F. (2019). Identifying the essential flood conditioning factors for flood prone area mapping using machine learning techniques. CATENA, 175, 174–192. https://doi.org/10.1016/j.catena.2018.12.011

Teng, J., Jakeman, A. J., Vaze, J., Croke, B. F. W., Dutta, D., & Kim, S. (2017). Flood inundation modelling: a review of methods, recent advances and uncertainty analysis. Environmental Modelling & Software, 90, 201–216. https://doi.org/10.1016/j.envsoft.2017.01.006

Terzaghi, K. (1939). Soil mechanics, a new chapter in engineering science. Journal of the Institution of Civil Engineers, 12, 106–141.

Tian, M., Zhang, D., Qu, G., Gao, L., Li, Y., Zhang, H., & Qiu, W. (2020). Research on influence zoning of tunnel side crossing existing urban roads based on ultimate shear strain failure criterion. IOP Conference Series: Materials Science and Engineering, 741(1), 012022. https://doi.org/10.1088/1757-899X/741/1/012022

Titti, G., Van Westen, C., Borgatti, L., Pasuto, A. & Lombardo, L. (2021). When enough is really enough? On the minimum number of landslides to build reliable susceptibility models. Geosciences, 11(11), 469.

Titti, G., Antelmi, M., Fusco, F., Longoni, L., & Borgatti, L. (2024). A new perspective for regional landslide susceptibility assessment. Italian journal of engineering geology and environment, 1(Special Issue 1), 275-283.

Trasforini, E., Campo, L., Ghizzoni, T., Libertino, A., Ottonelli, D., Ponserre, S., Rossi, L., & Rudari, R. (2024). Regional probabilistic flood displacement risk assessment: the Horn of Africa case study. EGU General Assembly 2024. https://doi.org/10.5194/egusphere-egu24-16971

Trigila, A., Iadanza, C., & Spizzichino, D. (2010). Quality assessment of the Italian Landslide Inventory using GIS processing. Landslides, 7, 455-470.

Tsubaki, R., & Kawahara, Y. (2013). The uncertainty of local flow parameters during inundation flow over complex topographies with elevation errors. Journal of Hydrology, 486, 71–87. https://doi.org/10.1016/j.jhydrol.2013.01.042

Tsubaki, R., Bricker, J. D., Ichii, K., & Kawahara, Y. (2016). Development of fragility curves for railway embankment and ballast scour due to overtopping flood flow. Natural Hazards and Earth System Sciences, 16, 2455–2472. https://doi.org/10.5194/nhess-16-2455-2016

Vafakhah, M., Mohammad Hasani Loor, S., Pourghasemi, H., & Katebikord, A. (2020). Comparing performance of random forest and adaptive neuro-fuzzy inference system data mining models for flood susceptibility mapping. Arabian Journal of Geosciences, 13(11), 417. https://doi.org/10.1007/s12517-020-05363-1

Volpi, E. (2019). On return period and probability of failure in hydrology. Wiley Interdisciplinary Reviews: Water, 6(3), e1340.

Wachs, M., & Kumagai, T. G. (1973). Physical accessibility as a social indicator. Socio-Economic Planning Sciences, 7(5), 437–456.

Wan, C. F., & Fell, R. (2008). Assessing the potential of internal instability and suffusion in embankment dams and their foundations. Journal of Geotechnical and Geoenvironmental Engineering, 134(3), 401–407. https://doi.org/10.1061/(ASCE)1090-0241(2008)134:3(401)

Wang, Z., Lai, C., Chen, X., Yang, B., Zhao, S., & Bai, X. (2015). Flood hazard risk assessment model based on random forest. Journal of Hydrology, 527, 1130–1141. https://doi.org/10.1016/j.jhydrol.2015.06.008

Wang, T., Teng, F., & Zhang, X. (2020). Assessing global and national economic losses from climate change: a study based on CGEM-IAM in China. Climate Change Economics, 11(3), 2041003. https://doi.org/10.1142/S201000782041003X

Wu (2020). Evaluation techniques for traffic safety of operating highway tunnels. E3S Web of Conferences. https://doi.org/10.1051/e3sconf/20

Yu, Y., Lv, M., Qian, J., Lv, J., & Miao, D. (2024). Fuzzy information gain ratio-based multi-label feature selection with label correlation. International Journal of Machine Learning and Cybernetics. https://doi.org/10.1007/s13042-023-02060-9

Zhao, G., Pang, B., Xu, Z., Yue, J., & Tu, T. (2018). Mapping flood susceptibility in mountainous areas on a national scale in China. Science of The Total Environment, 615, 1133–1142. https://doi.org/10.1016/j.scitotenv.2017.10.037

Zou, Z. B., Peng, H., & Luo, L. K. (2015). The Application of Random Forest in Finance. Applied Mechanics and Materials, 740, 947–951. https://doi.org/10.4028/www.scientific.net/AMM.740.947